Large-eddy Simulation of Turbulent Boundary Layer over Sinusoidal Hills and Multiscale Complex Topography

A DISSERTATION
SUBMITTED TO THE FACULTY OF THE GRADUATE SCHOOL
OF THE UNIVERSITY OF MINNESOTA
BY

Feng Wan

IN PARTIAL FULFILLMENT OF THE REQUIREMENTS
FOR THE DEGREE OF
Doctor of Philosophy

Fernando Porté-Agel

August, 2011

Acknowledgements

I would like to thank many people who helped me and inspired me during my life as a graduate student.

First and foremost, I want to thank my advisor Dr. Fernando Porté-Agel. He has shown me during these years what a true scholar is like. Passion, critical thinking, patience, all these attributes influenced me and will benefit me in the rest of my life. I appreciate his contributions of time and ideas, his support, both financially and mentally to make my Ph.D. life a valuable experience to me. Without his support, it would have been next to impossible to write this dissertation.

I am also grateful to my dissertation committee members: Dr. Heinz Stefan, Dr. Efi foufoula-Georgiou, and Dr. Krishnan Mahesh for their valuable advice and suggestions on my dissertation. My interactions with them both in their lectures and in some discussions have broadened my horizon and opened my view for various research topics that are outside my specific research area.

My fellow graduate students in the Saint Anthony Falls Lab also deserve my appreciation. Matt Carper, Rob Stoll and Qin Qian, who all gave me a lot of help and support like my older brothers and sisters, not only in my research but also in my personal life. Many other fellow students deserve thanks as well for making the lab an enjoyable working environment.

Last but not least, I want to express my gratitude to my family. My dear parents have worked so hard to provide my sister and I the best we could ever ask for. They have been unconditionally loving me and supporting me. Without their love, I would never have made it this far. I owe my sister Qinghua for her love, support and a lot of responsibilities to the family she assumed when I am here in the US. I thank my fiancé Jing for her support.

Dedication

To those who held me up over the years

Abstract

Atmospheric models require the parameterization of surface fluxes at regional scales. The accuracy of the parameterization relies on detailed information on the spatial and temporal distribution of turbulence in the atmospheric boundary layer (ABL). Large-eddy simulation (LES) has become an increasingly popular tool to study the ABL and obtain the three-dimensional transient information of the ABL. It uses a subgrid-scale (SGS) model to parameterize the subgrid turbulent transport. Here, three different SGS models are tested in LES of neutrally as well as stably stratified boundary layers over rough two-dimensional sinusoidal hills. The examined SGS models include the standard Smagorinsky model with a wall-matching function, the Lagrangian dynamic model, and the recently developed scale-dependent Lagrangian dynamic model. Simulation results obtained with different models are compared with turbulence statistics from wind tunnel experiments. We find that the scale-dependent Lagrangian dynamic model is able to dynamically (without any parameter tuning) capture the scale dependence of the model coefficient associated with regions of the flow with strong shear and/or thermal stratification. This scale-dependent dynamic procedure substantially improves the simulation results with respect to both the standard (non-dynamic) eddy-viscosity/diffusivity model and the scale-invariant dynamic model.

LES with the tested scale-dependent Lagrangian dynamic model is used to study neutral ABL flow over multiscale complex topography, which is generated using the restricted solid-on-solid (RSOS) model and able to capture the power-law scaling property of a -2 slope of elevation power spectrum in a log-log scale found in many natural landscapes. The parameterization needed to represent the effect of SGS topography in numerical models (e.g., coarser LESs or high-resolution weather models) of ABL flow is investigated. Specifically, the formulation of an effective roughness used to account for the increased aerodynamic roughness associated with SGS topography is proposed. Results from LESs performed using elevation fields pass-filtered at different spatial resolutions indicate a clear linear relation between the square of the effective roughness and the variance of elevation, and support the proposed formula.

High-resolution multiscale topography may not be directly represented in a LES of the ABL. One needs to spatially filter it to obtain a resolved topography to be directly used in LES and a SGS topography whose effect on the ABL needs to be parameterized. Here we propose a parameterization scheme of using a SGS roughness length in the lower boundary condition (the logarithmic law under neutral condition) in LES. The formulation of the SGS roughness length is proposed. The validity of the parameterization scheme is examined by simulating neutral ABL flow over a series of complex terrains that are filtered from a high-resolution multiscale topography at varying scales. Without applying the parameterization scheme in the series of simulations, the area-averaged velocity profiles over the series of terrains show clear discrepancies. After considering the parameterization of SGS topographic effect, that is, applying a SGS roughness length in the surface boundary condition, the velocity profiles show clear convergence and the validity of the parameterization scheme is proved.

Contents

List of Tables

List of Figures

Chapter 1

Introduction

The atmospheric boundary layer (ABL) is the lowest part of the troposphere that is in direct contact with the earth's surface. The height of the ABL varies in time and space, ranging from tens of meters in strongly statically stable situations, to several kilometers under convective conditions. The ABL is almost always turbulent, which makes the understanding of the ABL processes challenging.

The interactions between the ABL and the earth's surface (e.g., momentum, heat and water vapor fluxes) are important driving forces in weather and climate systems, and therefore attract a lot of attentions from researchers (e.g., [46, 41, 79, 77, 11]). Large-eddy simulation (LES), as a popular tool to study turbulence, has been extensively used to investigate the interaction between the ABL and topography (e.g., [79, 6, 11, 20, 31, 74, 75]). Despite its popularity, LES results are found to be sensitive to the determination of model coefficients in SGS models, which are used to parameterize the effect of unresolved eddies. The specification of SGS model coefficients is therefore one of the biggest challenges for LES. Many efforts have been made to improve the determination of SGS model coefficients (e.g., [23, 61, 68]). An important advancement is the dynamic procedure introduced by Germano et al. [23], which calculates the value of model coefficients at every time and position in the flow based on information from the smallest resolved scales and avoids the need for a priori specification or tuning of the model coefficient. Recently, Stoll and Porté-Agel [68] proposed the scale-dependent Lagrangian dynamic model, which relaxes the scale-invariance assumption of model coefficients in the standard dynamic model and assumes model coefficients have a power-law dependence with scale. In this research, we show that the scale-dependent Lagrangian dynamic model outperforms other commonly used SGS models (e.g., the standard eddy-viscosity/diffusivity model

and the scale-invariant dynamic model) in simulations of neutral [74] as well as stably-stratified [75] boundary-layer flow over sinusoidal hills.

Despite numerous LES studies of boundary layer turbulence over topography, few of them have focused on multiscale topography. Natural landscapes, however, often exhibit multiscale (often multifractal) structure, a high degree of self-similarity, and well-known scaling properties (e.g., [64]). For example, the power spectra of linear transects in many natural landscapes, when plotted on a log-log scale, show a clear -2 slope over a wide range of spatial scales, from a few meters up to tens of kilometers (e.g., [29, 56]). This remarkable scaling property of surface elevation fields of natural landscapes motivates us to explore possible scaling properties related to surface momentum fluxes of the atmospheric boundary layer (ABL) flow over natural topography. In this research, the restricted solid-on-solid (RSOS) model is used to generate multiscale complex surfaces that approximate natural landscapes. The elevation power spectrum of generated surfaces shows a clear scaling region with a -1.8 slope in a log-log scale. The slope is very close to that of natural landscapes, and it is therefore reasonable for us to use the generated surfaces to approximate natural landscapes. LES together with the scale-dependent Lagrangian dynamic model has been employed to simulate ABL flow over multiscale complex topography and investigate the parameterization of SGS topographical effect on the ABL in both a high-resolution weather model framework and a LES framework. The SGS topographic effect is accounted for by a SGS (effective) roughness length, and the formulation for the roughness length has been proposed. In the LES framework, the parameterization of SGS topographic effect is realized and validated by using the SGS roughness length in the LES lower boundary condition (the logarithmic law under neutral condition).

Each chapter in this thesis is a complete research article containing an abstract, introduction, numerical experiments, results and summary. In chapter 2, three SGS models have been tested in LES of neutral boundary layer over a rough two-dimensional sinusoidal hill. In chapter 3, we again test the three SGS models over a rough two-dimensional sinusoidal hill but in a stably-stratified boundary layer. Results from both chapter 2 and chapter 3 show that the scale-dependent dynamic procedure substantially improves the simulation results with respect to the standard eddy-viscosity/diffusivity model and the scale-invariant dynamic model. Chapter 4 covers the formulation of an effective roughness length of SGS topography in numerical models (e.g., high-resolution weather models) of ABL flow. A clear linear

relation between the square of the effective roughness and the variance of elevation is identified. Chapter 5 deals with the parameterization of SGS topographic effect in the LES. The parameterization is carried out by applying a SGS roughness length in the lower boundary condition (the logarithmic law) in LES. The unknown dimensionless coefficient in the SGS roughness length formulation is dynamically calculated in LES through a newly introduced model in which the dynamic procedure developed by Germano et al. [23] is employed and the area-averaged total surface stress is examined. The parameterization scheme is proven valid by results from simulating ABL flow over a series of complex terrains that are filtered from a high-resolution multiscale topography at varying scales.

Chapter 2

Evaluation of dynamic subgrid-scale models in large-eddy simulations of neutral turbulent flow over a two-dimensional sinusoidal hill

Abstract

Large-eddy simulation (LES) is used to simulate neutral turbulent boundary-layer flow over a rough two-dimensional sinusoidal hill. Three different subgrid-scale (SGS) models are tested: (a) the standard Smagorinsky model with a wall-matching function, (b) the Lagrangian dynamic model, and (c) the recently developed scale-dependent Lagrangian dynamic model [68]. The simulation results obtained with the different models are compared with turbulence statistics obtained from experiments conducted in the meteorological wind tunnel of the AES (Atmospheric Environment Service, Canada) [25]. We find that the scale-dependent dynamic model is able to account, without any tuning, for the local changes in the eddy-viscosity model coefficient. It can also capture the scale dependence of the coefficient associated with regions of the flow with strong mean shear and flow anisotropy. As a result, the scale-dependent dynamic model yields results that are more realistic than the ones obtained with the scale-invariant Lagrangian dynamic model.

2.1 Introduction

Large-eddy simulation (LES) can provide valuable high resolution spatial and temporal information necessary to understand the effects of topography on turbulent transport in the atmospheric boundary layer (ABL) (e.g., [40, 73, 21, 44, 25, 27, 10, 31]). LES explicitly resolves all scales of turbulent transport larger than the grid scale Δ (on the order of tens of meters in the ABL), while the smallest (less energetic) scales are parameterized using a subgrid-scale (SGS) model. Despite the

potential of LES, however, the strong spatial heterogeneity and flow anisotropy associated with topography hinder the performance of commonly used subgrid-scale models (e.g., [31, 32]).

Eddy-viscosity models are the most commonly used SGS models in LES of ABL flows. One of the main challenges in the implementation of these models is the specification of the model coefficients. Although the coefficients are well established for the case of isotropic turbulence (e.g. [67, 42, 23]), there is evidence from both simulations and experimental a-priori studies that these coefficients should decrease in regions of the flow with large flow anisotropy at the smallest resolved and subgrid scales associated with large local mean shear [17, 18, 30, 66, 28, 14, 62, 39, 60, 68].

One systematic approach to account for the spatial and temporal variability of the SGS model coefficient is the use of dynamic procedures [23, 24, 49], which consist of optimizing the value of the model coefficient at every position and time step by using information contained in the resolved scales and assuming scale invariance of the coefficient between the filter/grid scale and a slightly larger, test-filter scale. In order to guarantee numerical stability, these procedures require some kind of averaging. If the flow has directions of homogeneity, the averaging can be done over those directions (e.g., over horizontal planes in the case of flow over a flat homogeneous surface). For cases of flow over complex terrain, Lagrangian averaging (over flow pathlines) has been used in dynamic models [49]. The dynamic model has been found to yield unrealistic turbulence statistics (e.g. mean velocity profiles and turbulence spectra) in simulations of ABL flows over homogeneous [61] and heterogeneous [8, 68] flat surfaces, as well as flows over topography [31]. Iizuka and Kondo [31] tested the dynamic model and the Lagrangian dynamic model in simulations of a turbulent boundary layer over a two-dimensional hill. In comparisons with experimental wind-tunnel measurements of Ishihara et al. [33], the simulation results of Iizuka and Kondo [31] showed that the standard dynamic and Lagrangian dynamic models overestimated the time-averaged velocity near the surface over the hill crest. Porté-Agel et al. [61] showed that in simulations of neutral boundary layers over homogeneous surfaces, the dynamically computed coefficients are scale dependent, which is inconsistent with the assumption of scale invariance on which the dynamic procedure relies. Motivated by their results, Porté-Agel et al. [61] introduced the so-called scale-dependent dynamic model by relaxing the assumption of scale invariance of the model coefficient. The scale-dependent dynamic model was shown to overcome the limitations of the scale-invariant dynamic model in simulations of

neutral ABL flows over flat surfaces. More recently, a Lagrangian scale-dependent dynamic model version has been used in simulations of flow over heterogeneous surfaces [8, 68]. The performance of this model over topography has not been tested to date.

In this study, large-eddy simulation (LES) is used to simulate an experimentally well characterized turbulent boundary layer flow over a two-dimensional sinusoidal hill. Three different subgrid-scale (SGS) models are tested: (a) the standard Smagorinsky model with a wall-matching function, (b) the Lagrangian dynamic model, and (c) the recently developed Lagrangian dynamic scale-dependent model [68]. The simulation results obtained with the different models are compared with turbulence statistics obtained from experiments conducted in the meteorological wind tunnel of the AES (Atmospheric Environment Service, Canada) [25]. Next, a brief description of the three models is given.

2.1.1 The Smagorinsky model

The eddy-viscosity model is commonly used in LES to parameterize the SGS stresses τ_{ij} as

$$\tau_{ij} - \frac{1}{3}\delta_{ij}\tau_{kk} = -2\nu_T \widetilde{S}_{ij}, \tag{2.1}$$

where the tilde denotes spatial filtering using a three dimensional filter of size Δ, $\widetilde{S}_{ij} = \frac{1}{2}\left(\frac{\partial \widetilde{u}_i}{\partial x_j} + \frac{\partial \widetilde{u}_j}{\partial x_i}\right)$ is the resolved (filtered) strain rate tensor, and ν_T is the eddy viscosity, which is defined as [67]

$$\nu_T = [C_S\Delta]^2 \left|\widetilde{S}\right|, \tag{2.2}$$

where $\left|\widetilde{S}\right| = \left(2\widetilde{S}_{ij}\widetilde{S}_{ij}\right)^{\frac{1}{2}}$ is the magnitude of the resolved strain-rate tensor, and C_S is a non-dimensional parameter called the Smagorinsky coefficient. The value of the model parameter C_S is well established for isotropic, homogeneous turbulence with cutoff in the inertial subrange and Δ equal to the grid size ($C_S \sim 0.17$, [42]). However, anisotropy of the flow due to strong mean shear near the surface makes the optimum value of C_S depart from its isotropic counterpart. A decrease in the Smagorinsky coefficient is associated with an increase in anisotropy in both the resolved and SGS velocities [17, 18, 30, 66, 28, 14, 62, 39, 60, 68]. In order to account for these effects, application of eddy-diffusion models in LES of the ABL has often involved the use of various types of *ad hoc* wall damping corrections. For

example, Mason and Thomson [47] proposed to use the equation

$$\frac{1}{\lambda^n} = \frac{1}{\lambda_o^n} + \frac{1}{[\kappa(z+z_o)]^n}, \tag{2.3}$$

where $\kappa(\approx 0.4)$ is the von Karman constant, $\lambda = C_S\Delta$ is the length scale in the model, $\lambda_o = C_o\Delta$ is the length scale far from the wall, z_o is the roughness length, and C_o and n are adjustable parameters. They apply this formulation with different values of C_o (from about 0.1 to 0.3) and n (1, 2, and 3).

2.1.2 The Lagrangian dynamic model

The dynamic procedure [23] provides a systematic way to calculate the value of the model coefficient (C_S^2) at every time and position in the flow based on the dynamics of the smallest resolved scales. The model is based on the Germano identity

$$L_{ij} = T_{ij} - \bar{\tau}_{ij} = \overline{\widetilde{u}_i\widetilde{u}_j} - \overline{\widetilde{u}}_i\overline{\widetilde{u}}_j, \tag{2.4}$$

where L_{ij} is the so-called Leonard stress tensor that can be calculated based on the resolved scales, and T_{ij} is the SGS stress at a test filter scale $\bar{\Delta}$ (typically $\bar{\Delta} = 2\Delta$). The overbar denotes a spatial filtering operation at scale $\bar{\Delta}$.

Applying the Smagorinsky model at the test filter scale yields the following equation

$$T_{ij} - \frac{1}{3}\delta_{ij}T_{kk} = -2(C_S(\bar{\Delta})\bar{\Delta})^2|\overline{\widetilde{S}}|\overline{\widetilde{S}}_{ij}. \tag{2.5}$$

Substituting equations 2.1 and 2.5 into 2.4 and assuming scale invariance of the model coefficient, i.e.,

$$C_S^2(2\Delta) = C_S^2(\Delta), \tag{2.6}$$

results in the equations describing the error associated with the use of the Smagorinsky model in the Germano identity

$$e_{ij} = L_{ij} - \frac{1}{3}\delta_{ij}L_{kk} - C_S^2(\Delta)M_{ij}, \tag{2.7}$$

where

$$M_{ij} = 2\Delta^2(\overline{|\widetilde{S}|\widetilde{S}_{ij}} - 4|\overline{\widetilde{S}}|\overline{\widetilde{S}}_{ij}). \tag{2.8}$$

Optimizing the value of C_S^2 through least squares minimization of the error given by equation 2.7 [43, 24] leads to

$$C_S^2 = \frac{\langle L_{ij}M_{ij}\rangle}{\langle M_{ij}M_{ij}\rangle}. \tag{2.9}$$

In order to implement the dynamic model, some sort of averaging (denoted with brackets $\langle\ \rangle$ in equation 2.9) needs to be used to guarantee numerical stability of the procedure. Typically averaging is done over directions of flow homogeneity (e.g., horizontal planes over flat homogeneous terrain), or over flow pathlines using the Lagrangian averaging procedure developed by Meneveau et al. [49]. Lagrangian dynamic models are therefore suitable for simulations of the ABL over complex terrain, where there is no direction of homogeneity in the flow. More detailed descriptions of the Lagrangian dynamic procedure can be found in Stoll and Porté-Agel [68].

The dynamic model avoids the need for a-priori specification or tuning of the coefficient because it is evaluated directly from the resolved scales in the LES. However, recent studies have shown that the dynamic models have problems to reproduce the correct flow statistics over both flat surfaces [61] as well as complex terrain [31].

2.1.3 The Lagrangian scale-dependent dynamic model

Recently, Porté-Agel et al. [61] proposed a scale-dependent dynamic model, a modification of the dynamic procedure that allows the model coefficient to change with scale (i.e. not assuming that $C_S^2(\Delta) = C_S^2(2\Delta)$). We can still write down the Germano identity for the Smagorinsky model. However, now M_{ij} also depends on the ratio of the model coefficient at the test filter scale and the filter scale [48]

$$M_{ij} = 2\Delta^2(\overline{|\widetilde{S}|\widetilde{S}_{ij}} - 4\frac{C_S^2(2\Delta)}{C_S^2(\Delta)}\overline{|\widetilde{S}|}\,\overline{\widetilde{S}_{ij}}). \tag{2.10}$$

We now introduce a new variable $\beta = C_S^2(2\Delta)/C_S^2(\Delta)$. To obtain a dynamic value for β, we use a second test filter at another scale larger than Δ, e.g. $\widehat{\Delta} = 4\Delta$, and denote variables filtered at scale 4Δ by a caret. By using the second test filter, the error associated with the use of the Smagorinsky model in the Germano identity between Δ and $\widehat{\Delta}$ now becomes

$$e'_{ij} = L'_{ij} - \frac{1}{3}\delta_{ij}L'_{kk} - C_S^2(\Delta)M'_{ij}, \tag{2.11}$$

where

$$L'_{ij} = \widehat{\widetilde{u}_i\widetilde{u}_j} - \widehat{\widetilde{u}}_i\widehat{\widetilde{u}}_j \tag{2.12}$$

$$M'_{ij} = 2\Delta^2(\widehat{|\widetilde{S}|\widetilde{S}_{ij}} - 4^2\beta^2\widehat{|\widetilde{S}|}\,\widehat{\widetilde{S}}_{ij}). \tag{2.13}$$

Comparing with the original scale invariant assumption, a much weaker assumption is made that

$$C_S^2(2\Delta)/C_S^2(\Delta) = C_S^2(4\Delta)/C_S^2(2\Delta) \tag{2.14}$$

and therefore

$$\beta^2 = \frac{C_S^2(4\Delta)}{C_S^2(\Delta)}. \tag{2.15}$$

The same method used with the first test filter is employed here to minimize the error in equation 2.11 locally backward along the fluid path line, resulting in another equation for $C_S^2(\mathbf{x}, t)$.

$$C_S^2(\mathbf{x}, t) = \frac{\left\langle L'_{ij} M'_{ij} \right\rangle}{\left\langle M'_{ij} M'_{ij} \right\rangle}, \tag{2.16}$$

where, in the case of the Lagrangian scale-dependent dynamic model, the brackets $\langle$ $\rangle$ denote averaging along fluid pathlines. Setting equation 2.16 equal to equation 2.9 results in a single equation from which the unknown scale dependence parameter $\beta(\mathbf{x}, t)$ may be obtained dynamically. For more details on the Lagrangian scale-dependent dynamic procedure, see Stoll and Porté-Agel [68].

By using information on the dynamics of the flow corresponding to an additional test-filter scale (e.g. 4Δ), the scale-dependent model has the ability to detect and account for scale dependence in a dynamic manner (based on the information of the resolved field and, thus, not requiring any tuning of parameters). In particular, the scale-dependent dynamic model is used to dynamically calculate not only $C_S^2(\Delta)$, but also the value of the scale-dependence coefficient $\beta = C_S^2(2\Delta)/C_S^2(\Delta)$. Lagrangian scale-dependent dynamic models have successfully been implemented in simulations of ABLs over flat heterogeneous terrain [8, 68]. In this paper, we study the performance of the Lagrangian scale-dependent dynamic model in simulations of a boundary layer over rough two dimensional sinusoidal hills.

2.2 Numerical experiments

The large-eddy simulation code is a modified version of the code described by Albertson and Parlange [1], Porté-Agel et al. [61], and Stoll and Porté-Agel [68]. The code uses a mixed pseudospectral finite-difference method, i.e., spatial derivatives are computed using pseudospectral methods in the horizontal directions and finite differences in the vertical direction. Consequently, the boundary conditions in the

horizontal directions are periodic. A second-order Adams-Bashforth scheme is used for time advancement. The upper boundary condition is a fixed stress-free lid. The lower boundary condition consists of using similarity theory (the logarithmic law) to calculate the instantaneous (filtered) surface shear stress as a function of the velocity field at the lowest computational level. In particular, the two components of the surface shear stress vector are calculated following

$$\tau_{xz} = -C_d \widetilde{V}(\widetilde{u}\ cos\theta_x + \widetilde{w}\ sin\theta_x) \tag{2.17}$$

$$\tau_{yz} = -C_d \widetilde{V}(\widetilde{v}\ cos\theta_y + \widetilde{w}\ sin\theta_y) \tag{2.18}$$

where C_d is the drag coefficient obtained from the logarithmic law. $\widetilde{u}$, $\widetilde{v}$ and $\widetilde{w}$ are the filtered streamwise, spanwise and vertical velocities, and $\widetilde{V}$ is the magnitude of the tangential velocity, all calculated at the lowest computational grid level. θ_x and θ_y are the local angles of inclination of the topography in the x and y direction, respectively ($\theta_y = 0$, in our case).

The simulated physical domain corresponds to the space above two sinusoidal waves with non-dimensional elevation

$$z_s/L_z = a\ \cos(2x/L_z), \tag{2.19}$$

where $a = 0.249$ is the normalized wave amplitude, x/L_z is the normalized streamwise position, and L_z is the lenght scale used for normalization (see Figure 2.1). The flow direction is perpendicular to the wave crests. The coordinate transformation developed by Clark [15] has been used to transform the sinusoidal wave bounded physical domain into a rectangular computational domain. The transformation is a terrain following transformation and takes the following form:

$$\bar{z} = H(z - z_s)/(H - z_s) \tag{2.20}$$

where $\bar{z}$ is the vertical position in the transformed system. z_s and H denote the actual elevation (in the original system) of the terrain and the top of the domain, respectively. In order to match the wind-tunnel experimental conditions of Gong et al. [25], the computational domain, after normalization with the length scale $L_z = 194$ mm, is of size (2π, 2π, π). The non-dimensional surface roughness is set to $z_o/L_z = 2.06 \times 10^{-3}$. The computational domain is divided into $80 \times 80 \times 80$ uniformly spaced grid points. The grid is staggered in the vertical direction, with the vertical velocity stored halfway between the other variables. Wind velocities are normalized using the free stream wind tunnel velocity, $U_o = 10$ m/s.

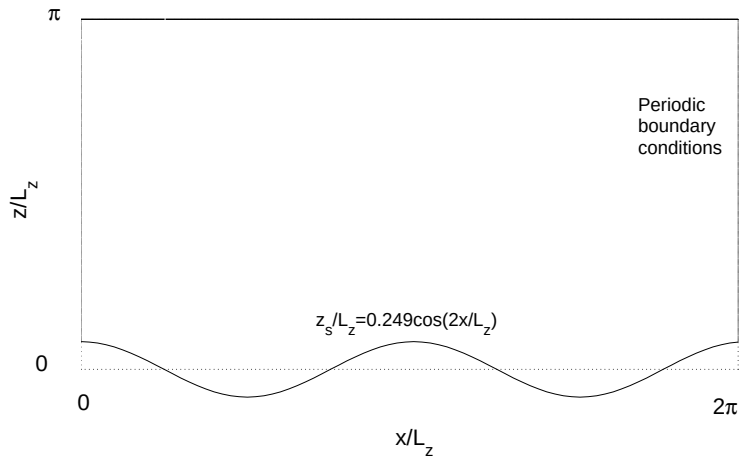

Figure 2.1: Schematic of computational domain over the sinusoidal hill

A horizontal pressure gradient is exerted on the flow in the streamwise direction. The magnitude of this pressure gradient is set to balance the drag forces (surface stress and form drag) measured during the experiment [25]. The value of the non-dimensional pressure gradient is 0.654. The simulations are run for a period of time long enough to guarantee quasi-steady flow conditions and statistical convergence of the results presented in the next section.

2.3 Results

Figures 2.2 (a) through 2.2 (d) show the simulated non-dimensional streamwise velocity profiles obtained above four different streamwise positions in a wave: the wave crest (Figure 2.2 (a)), 1/4 wavelength downwind of the crest (Figure 2.2 (b)), the wave trough (Figure 2.2 (c)), and 1/4 wavelength upwind of the crest (Figure 2.2 (d)). The results are averaged over time and over the spanwise direction and they are non-dimensionalized with the free stream velocity U_o. Different lines correspond to the different SGS models under consideration: the Smagorinsky model with two different matching functions (SMAG-1: $Co = 0.17$ and $n = 1$; and SMAG-2: $Co = 0.1$ and $n = 1$ in equation 2.3), the Lagrangian Dynamic model, and the Lagrangian Scale-Dependent Dynamic model. Results are compared with wind tunnel data (symbols) of Gong et al. [25]. From Figure 2.2 (a) we find that the Lagrangian

dynamic model clearly overestimates the average velocity near the surface by as much as 20%. This behavior of the velocity profile over the hill crest obtained with the Lagrangian dynamic model is consistent with the velocity overestimation of about 25% reported by Iizuka and Kondo [31] in their large-eddy simulations of flow over a single two-dimensional hill using the same SGS model. The results from the Smagorinsky model show substantial sensitivity to the choice of parameters and, consequently, the shape of the matching function. The scale-dependent dynamic procedure, which retains the advantage of dynamic models of not requiring any parameter tuning, substantially improves the simulation results with respect to the scale-invariant dynamic model.

The simulated velocity profiles at 1/4 wavelength downwind of the wave crest (Figure 2.2 (b)) and in the wave trough (Figure 2.2 (c)) show relatively small sensitivity to the SGS model, compared with the results over the wave crest (Figure 2.2 (a)). The simulated velocities are close to the measurements above a height of about 30 mm in Figure 2.2 (b) and about 50 mm in Figure 2.2 (c). Note that the region below those heights, as reported in Gong et al. [25], corresponds to the upper limit of a flow recirculation zone that develops downwind of the wave crest. In the recirculation zone, mean velocities are negative and cannot be accurately measured by the hot-wire anemometer, which cannot distinguish between positive and negative velocities and is succeptible to large errors due to flow distortion by the probe support.

The simulated average velocity 1/4 wavelength upwind of the crest (Figure 2.2 (d)) is slightly underestimated by the Smagorinsky model with matching function in the near-surface region, while it is slightly overestimated by the Lagrangian dynamic model at heights between 30 mm and 200 mm. The scale-dependent Lagrangian dynamic model gives a reasonable prediction throughout most of the domain.

The non-dimensional standard deviations of the resolved streamwise, transverse and vertical velocities over the wave crests are presented in Figure 2.3 (a), Figure 2.3 (b) and Figure 2.3 (c), respectively. Results are again compared with the wind tunnel experimental data (symbols) of Gong et al. [25]. Like in the case of the mean velocity profiles, the standard deviations of the horizontal velocity components simulated with the Smagorinsky model show strong sensitivity to the choice of the matching function for the eddy viscosity coefficient. The Lagrangian dynamic model overpredicts by as much as 50% the level of fluctuations of the horizontal velocity components and also the vertical velocity component. The overestimation of the

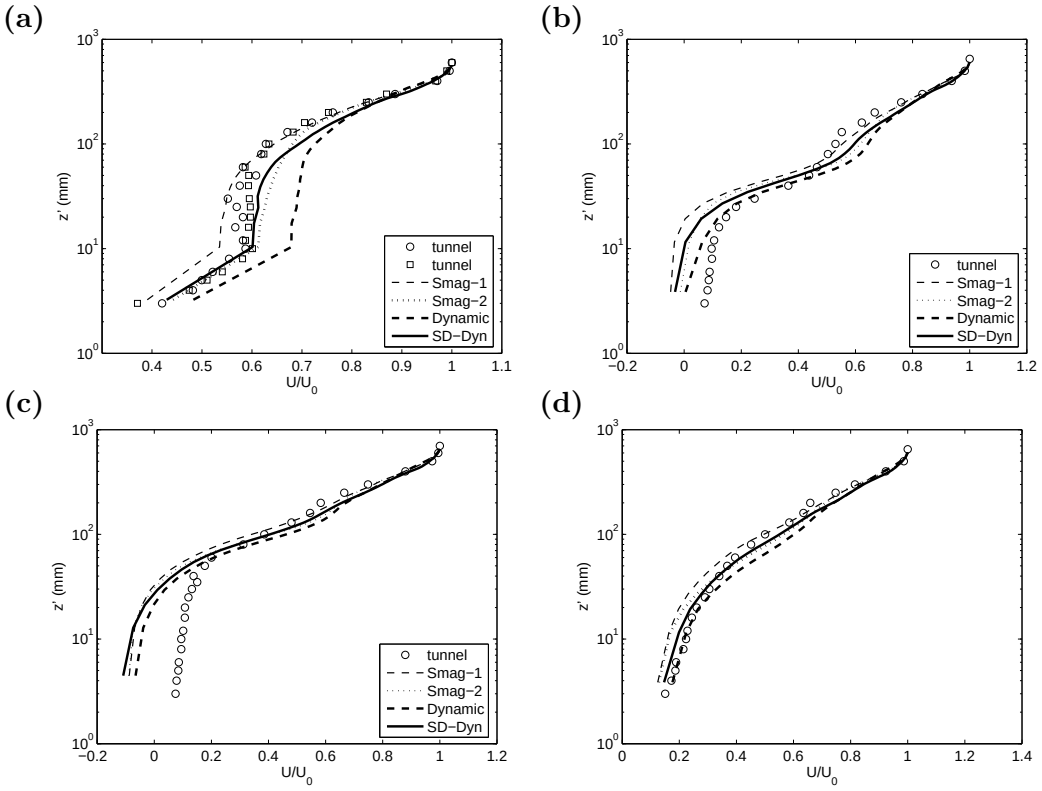

Figure 2.2: Non-dimensional velocity profiles from wind tunnel data (symbols) and from LES with different SGS models: Smagorinsky model with two different matching functions (thin dashed and dotted lines), dynamic model (dashed line), and scale-dependent dynamic model (solid line). Results are presented for different positions in the flow: over the wave crests (a); over 1/4 wavelength downwind of the crest (b); over the wave trough (c); and over 1/4 wavelength downwind of the trough (d).

resolved velocity variance is consistent with the idea that the dynamic model is not dissipative enough, and it is in good agreement with previous studies over flat terrain [61, 8]. The Lagrangian scale-dependent dynamic model improves the results with respect to its scale-invariant counterpart, though still overestimating the level of fluctuations of the velocity field.

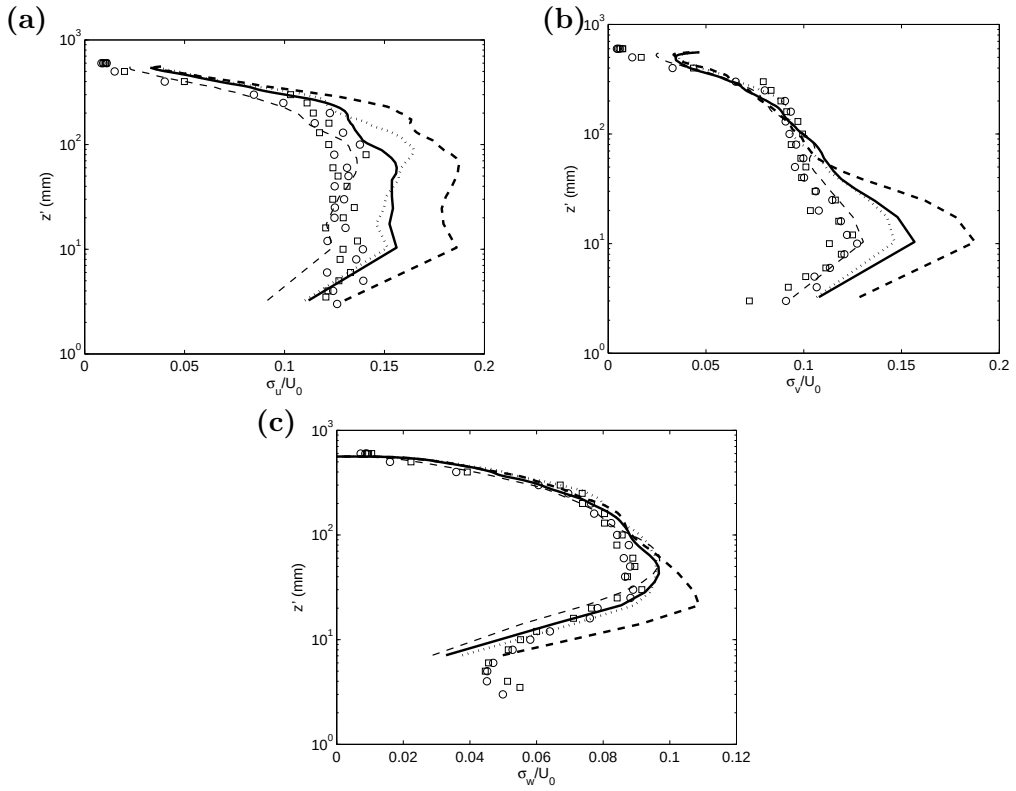

Figure 2.3: Non-dimensional standard deviation of the resolved velocities from wind tunnel data (symbols) and from LES with different SGS models: Smagorinsky model with two different matching functions (thin dashed and dotted lines), dynamic model (dashed line), and scale-dependent dynamic model (solid line). Results are presented over the wave crests: (a) standard deviation of streamwise velocity; (b) standard deviation of spanwise velocity; (c) standard deviation of vertical velocity.

In order to illustrate the resolution sensitivity of the simulation results, mean velocity profiles over the hill crest, obtained with the scale-invariant and scale-dependent dynamic models, are presented in Figures 2.4 (a) and 2.4 (b), respectively. The results from the scale-invariant dynamic model show clear resolution dependence, in contrast with the smaller resolution effects obtained with the scale-dependent dynamic model. Similar differences in the resolution effects (not shown

here) are found for the simulation results at other locations in the flow.

The dynamically calculated values of the model coefficient C_S^2 obtained using the Lagrangian dynamic and Lagrangian scale-dependent dynamic models are presented in Figures 2.5 and 2.6, respectively. As expected, for any given horizontal position, both coefficients decrease as the distance to the surface decreases in order to account for the reduction in the characteristic scale of the turbulence near the surface. In addition, there is a clear dependence of the coefficient on horizontal position, associated with the strong non-homogeneity of the flow. For the same distance to the ground, the coefficient is smaller near the crest, where the flow undergoes strong straining. Alternatively, the coefficient is larger in the downwind of the crest, where the flow detaches from the surface (recirculation region) and is subject to smaller strain rates. It is important to note that the value of the coefficient is substantially larger for the scale-dependent dynamic model. The larger value of C_S, together with the increased mean velocity gradients, results in a larger transfer of kinetic energy from the resolved to the sub-grid scales (SGS dissipation). An overestimation in the rate of removal of energy from the resolved scales leads, in turn, to smaller values of the standard deviations of the resolved velocity, as shown in Figure 2.3 (a), 2.3 (b) and 2.3 (c). Similar trends in the values of the model coefficient, mean velocity and resolved kinetic energy fields were also reported by Porté-Agel et al. [61] in simulations of a neutral boundary layer using both scale-invariant and scale-dependent dynamic model.

Figure 2.7 shows the value of the scale dependence parameter β obtained dynamically with the Lagrangian scale-dependent dynamic model. The value of β is close to 1 away from the surface, where the flow is more isotropic at the smallest resolved and subgrid scales and, consequently, C_S^2 is scale invariant. β becomes smaller as the surface is approached due to increased shear and anisotropy of the flow. The smallest values of β are found near the crest, particularly in the upwind side, where the mean shear and anisotropy of the flow are stronger.

2.4 Summary

Large-eddy simulation (LES) has been used to simulate neutral turbulent boundary-layer flow over a rough two-dimensional sinusoidal hill. Three different subgrid-scale (SGS) models are tested: *(a)* the standard Smagorinsky model with a wall-matching

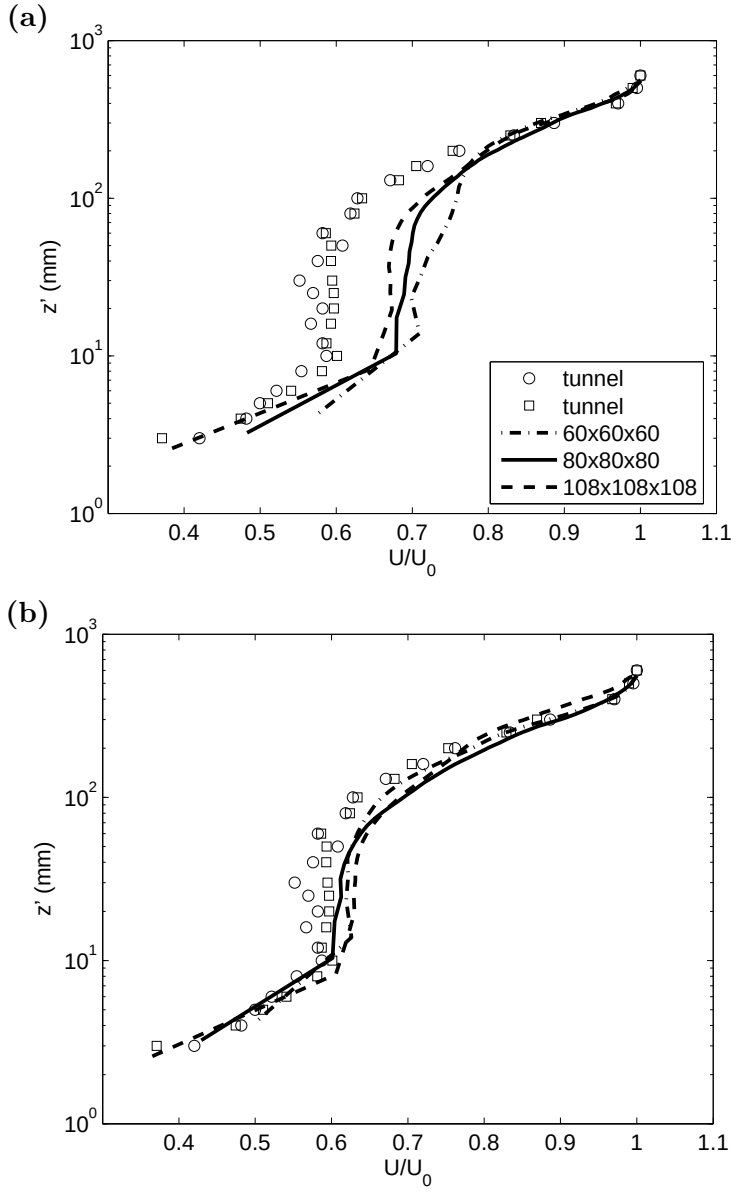

Figure 2.4: Effect of grid resolution on the simulated non-dimensional velocity profile over the wave crest obtained with the Lagrangian dynamic model (a) and the scale-dependent Lagrangian dynamic model (b). The wind tunnel data of Gong et al. (1996) (symbols) are also shown.

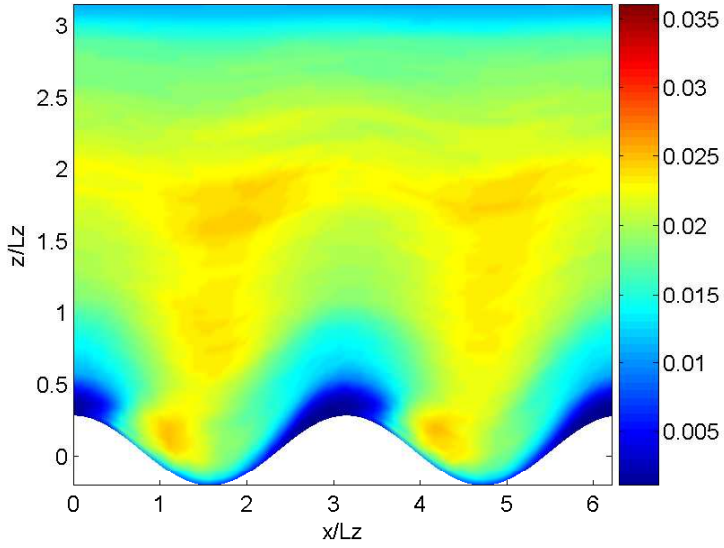

Figure 2.5: Smagorinsky coefficient (C_S^2) obtained with the Lagrangian dynamic model. Results are averaged over time and spanwise direction.

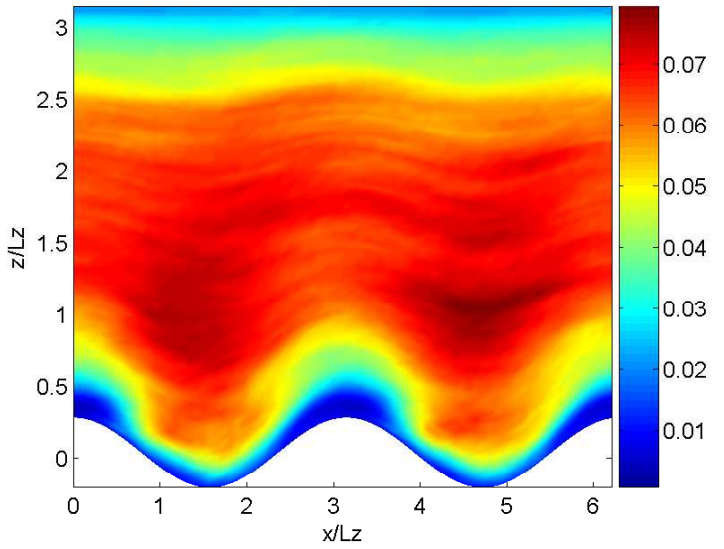

Figure 2.6: Smagorinsky coefficient (C_S^2) obtained with the Lagrangian scale-dependent dynamic model. Results are averaged over time and spanwise direction.

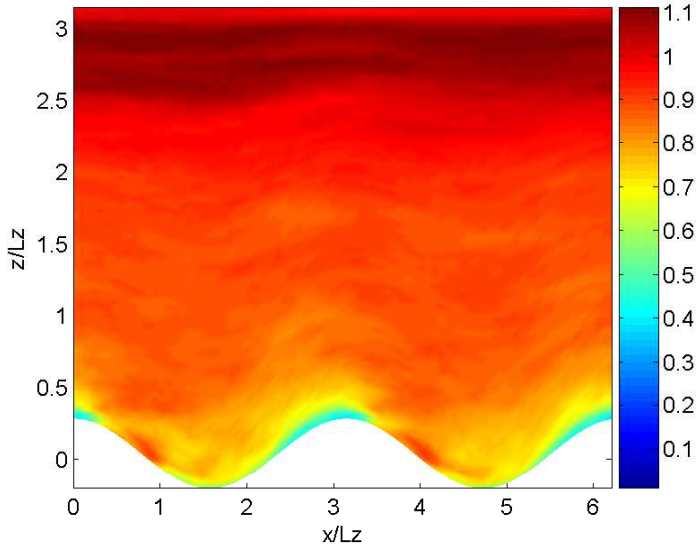

Figure 2.7: Scale dependence parameter (β) obtained with the Lagrangian scale-dependent dynamic model. Results are averaged over time and spanwise direction.

function, *(b)* the Lagrangian dynamic model, and *(c)* the recently developed scale-dependent Lagrangian dynamic model [68]. The simulation results obtained with the different models are compared with turbulence statistics obtained from experiments conducted in the meteorological wind tunnel of the Atmospheric Environment Service of Canada [25].

The dynamic models have the important advantage of providing tuning-free simulations since the model coefficient is calculated based on the dynamics of the resolved flow. However, the flow simulated using the Lagrangian dynamic model shows important differences compared with the wind tunnel experimental data. In particular, the Lagrangian dynamic model is not dissipative enough, leaving too much kinetic energy in the resolved flow. The model overestimates the magnitude of the velocity over the wave crests by about 20%, which is in agreement with the simulation results of Iizuka and Kondo [31] in simulations over a single two-dimensional hill.

By relaxing the assumption of scale invariance in the dynamic model, the scale-dependent dynamic model [61, 68] is able to dynamically (without any parameter tuning) capture the scale dependence of the model coefficient using information of

the smallest resolved scales. Our results show that this procedure substantially improves the simulation results with respect to the scale-invariant dynamic model.

Chapter 3

Large-Eddy Simulation of Stably-Stratified Flow Over a Steep Hill

Abstract

Large-eddy simulation (LES) is used to simulate stably-stratified turbulent boundary-layer flow over a steep two-dimensional hill. To parameterize the subgrid-scale (SGS) fluxes of heat and momentum, three different types of SGS models are tested: (a) the Smagorinsky model, (b) the Lagrangian dynamic model, and (c) the scale-dependent Lagrangian dynamic model [68]. Simulation results obtained with the different models are compared with data from wind tunnel experiments conducted at the Environmental Flow Research Laboratory (EnFlo), University of Surrey, U.K. [65]. It is found that, in this stably-stratified boundary-layer flow simulation, the scale-dependent Lagrangian dynamic model is able to account for the scale dependence of the eddy-viscosity and eddy-diffusivity model coefficients associated with flow anisotropy in flow regions with large mean shear and/or strong flow stratification. As a result, simulations using this tuning-free model lead to turbulence statistics that are more realistic than those obtained with the other two models.

3.1 Introduction

Large-eddy simulation (LES) has become a popular tool to study turbulent atmospheric boundary-layer (ABL) flows over topography. In particular, several LES studies have investigated the effect of topography on boundary layer turbulence under neutral stratification conditions (e.g., [10, 12, 25, 27, 31, 74]). To this date, however, only a few studies have used LES to study stably-stratified boundary-layer flows over topography (e.g., [13]), and not much is known about the accuracy of the LES technique and subgrid-scale (SGS) models in simulations of this type of flow.

Considering the sensitivity of LES results to SGS parameterizations in simulations of neutral boundary layers over topography (e.g., [31, 74]) and stable boundary layers over flat terrain (e.g., [5, 69]), one expects the combined effects of topography and atmospheric stability to pose an important challenge to SGS models in LES.

LES resolves scales of turbulent transport larger than the grid/filter scale Δ , and parameterizes smaller (subgrid) scales using a SGS model. The most commonly used SGS models in LES of ABL flows are the eddy-viscosity model for the SGS stresses and the eddy-diffusivity model for the SGS scalar fluxes. The specification of SGS model coefficients is one of the biggest challenges for LES as it has been found to have an important effect on the performance of the SGS models and, as a result, on the accuracy of the simulations. SGS coefficients are well established for homogeneous, isotropic turbulence (e.g., [42, 45]). However, in flow regions with strong anisotropy at the smallest resolved and subgrid scales, the coefficients in the eddy-viscosity and eddy-diffusivity models are found to deviate from the well-established isotropic values (e.g., [4, 14, 16, 28, 39, 51, 59, 62, 60, 68]). In particular, the optimal values of those coefficients have to decrease in order to account for the local reduction in the characteristic length scales of the turbulence associated with increased mean shear near the surface (e.g., [39, 68]) and/or increased atmospheric stability (e.g., [39, 62]).

The dynamic procedure provides a systematic approach to specify the values of the SGS coefficients in the eddy-viscosity and eddy-diffusivity models [23, 43, 52]. It does not require parameter specification or tuning, and model coefficients are optimized at every position and time step based on information from the resolved scales with the assumption that the coefficients are scale invariant in a range of scales between the filter/grid scale and a slightly larger test filter scale. In simulations of neutral ABL flows over homogeneous surfaces, Porté-Agel et al. [61] found that the dynamically calculated model coefficients showed dependence on resolution (filter scale), which is against the underlying assumption of scale invariance made in the dynamic model. With this unreasonable assumption, the standard dynamic model has been shown to yield model coefficients that are too low. This, in turn, leads to an accumulation of energy at high wavenumbers and explains why the dynamic model is not dissipative enough and yields inaccurate turbulence statistics in simulations of ABL flows over homogeneous [61] and heterogeneous [8, 68] flat surfaces, as well as neutral boundary-layer flows over topography [31, 74]. Motivated by those results, Porté-Agel et al. [61] and Porté-Agel [60] introduced the scale-dependent

dynamic model, which is used to compute dynamically not only the value of the model coefficients in the eddy-viscosity and eddy-diffusivity models, respectively, but also the dependence of these coefficients with scale. To achieve that, the scale-dependent dynamic model assumes a power-law dependence of the coefficient with scale. It is important to note that this power-law dependence is only applied to a small range of resolved scales (between the filter scale and a test filter scale) and has been shown to be a realistic assumption in a priori field studies [9, 63]. Simulations of neutral boundary-layer flows over both flat surfaces [8, 61, 60, 68] and simple topography [74] have shown that the scale-dependent dynamic model improves the level of SGS dissipation (rate of energy transfer from the resolved to the subgrid scales), which results in more realistic simulated velocity and scalar statistics.

In order to ensure numerical stability, the application of the dynamic and scale-dependent dynamic models requires some sort of averaging. For flows with directions of homogeneity, the averaging can be done over those directions (e.g., over horizontal planes in the case of flow over a flat homogeneous surface). For cases of flow over complex terrain, Lagrangian averaging (over flow pathlines) has been used in the Lagrangian dynamic model [49] as well as the scale-dependent Lagrangian dynamic model [68].

In this paper, we test the performance of three SGS models in simulations of stable boundary-layer flow over a single steep hill against laboratory experiments. These models are: (a) the Smagorinsky model, (b) the Lagrangian dynamic model, and (c) the recently developed scale-dependent Lagrangian dynamic model [68]. Next, a brief description of the three models is given.

3.1.1 The Smagorinsky model

The SGS stress τ_{ij} is commonly parameterized using an eddy-viscosity model of the form [67]:

$$\tau_{ij} - \frac{1}{3}\delta_{ij}\tau_{kk} = -2\nu_T \widetilde{S}_{ij}, \tag{3.1}$$

$$\nu_T = [C_S \Delta]^2 \left|\widetilde{S}\right|, \tag{3.2}$$

where τ_{ij} is the SGS stress at filter (grid) scale, $\widetilde{S}_{ij} = \frac{1}{2}\left(\frac{\partial \widetilde{u}_i}{\partial x_j} + \frac{\partial \widetilde{u}_j}{\partial x_i}\right)$ is the resolved strain-rate tensor, ν_T is the eddy viscosity, $\left|\widetilde{S}\right| = \left(2\widetilde{S}_{ij}\widetilde{S}_{ij}\right)^{\frac{1}{2}}$ is the magnitude of

the resolved strain-rate tensor, C_S is the Smagorinsky coefficient, and Δ is the size of the spatial filter.

The value of the Smagorinsky coefficient C_S is well established for isotropic and homogeneous turbulence ($C_S \sim 0.17$, [42]). The reduction of characteristic length scale and flow anisotropy near the surface, however, makes the optimal value of the Smagorinsky coefficient depart from its isotropic counterpart (e.g., [4, 16, 51, 59]). To account for this effect, Mason and Thomson [47] proposed the following formula:

$$\frac{1}{\lambda^n} = \frac{1}{\lambda_o^n} + \frac{1}{[\kappa(z+z_o)]^n}, \tag{3.3}$$

where κ (≈ 0.4) is the von Karman constant, $\lambda = C_S\Delta$ is the length scale in the model, $\lambda_o = C_o\Delta$ is the length scale far from the wall, z_o is the roughness height, and C_o and n are adjustable parameters. C_o generally takes values between 0.1 and 0.3, and n is an integer often chosen to be 1, 2 or 3. In this study, the values of C_o and n are set to be 0.1 and 1, respectively. Recent field experiments [39, 62] and numerical simulations using dynamic models [38] have shown that the optimal value of the Smagorinsky coefficient decreases with increasing stability in order to account for the reduction of turbulence eddy sizes as well as characteristics length scales associated with thermal stratification. Even though some empirical formulations have been proposed to account for this effect [39], they are usually based on horizontally-averaged variables and thus are not easily applicable to simulations of heterogeneous boundary layers.

To parameterize the SGS scalar flux q_i, the eddy-diffusivity model is typically used:

$$q_i = -D_T \frac{\partial \tilde{\theta}}{\partial x_i}, \tag{3.4}$$

$$D_T = C_S^2 Pr_{sgs}^{-1} \Delta^2 \left|\widetilde{S}\right|, \tag{3.5}$$

where q_i denotes SGS scalar flux at filter (grid) scale, D_T is the eddy diffusivity, $C_S^2 Pr_{sgs}^{-1}$ is a lumped eddy-diffusivity coefficient composed of the Smagorinsky coefficient and the SGS Prandtl number Pr_{sgs}. A value of 0.4 is often used for the SGS Prandtl number in neutral turbulent flows [34] as well as thermally stratified boundary layers [38]. In this study, the value of the SGS Prandtl number is set to be 0.4 as well. However, it is important to note that recent experimental (e.g., [39, 62]) and numerical (e.g., [5, 69]) studies have shown that Pr_{sgs} should increase

with increasing atmospheric stability. This effect further contributes (together with the above-mentioned decrease in C_S) to a reduction in the lumped eddy-diffusivity coefficient and the model length scale in thermally stratified regions of the flow.

3.1.2 The Lagrangian dynamic model

The dynamic procedure [23] optimizes the value of the Smagorinsky coefficient (C_S^2) using the information from the smallest resolved scales without the need for parameter tuning. The Germano identity is introduced as

$$L_{ij} \equiv T_{ij} - \bar{\tau}_{ij} = \overline{\widetilde{u}_i \widetilde{u}_j} - \overline{\widetilde{u}}_i \overline{\widetilde{u}}_j, \tag{3.6}$$

In the above equation, L_{ij} is a resolved stress tensor, also referred to as the Leonard stress, and T_{ij} is the SGS stress at a test filter scale $\bar{\Delta}$ (typically $\bar{\Delta} = 2\Delta$). The overbar in equation 3.6 denotes a spatial filtering operation at scale $\bar{\Delta}$. T_{ij} can be calculated using the eddy-viscosity model

$$T_{ij} - \frac{1}{3}\delta_{ij} T_{kk} = -2(C_S(\bar{\Delta})\bar{\Delta})^2 \left|\overline{\widetilde{S}}\right| \overline{\widetilde{S}}_{ij}, \tag{3.7}$$

where $C_S(\bar{\Delta})$ denotes the Smagorinsky coefficient at the test filter scale $\bar{\Delta}$. Substituting the SGS stresses at scale $\bar{\Delta}$ (equation 3.7) and scale Δ (equation 3.1) into the Germano identity, one can calculate the error incurred by using the Smagorinsky model in the Germano identity as

$$e_{ij} = L_{ij} - \frac{1}{3}\delta_{ij} L_{kk} - C_S^2(\Delta) M_{ij}, \tag{3.8}$$

where

$$M_{ij} = 2\Delta^2 (\overline{\left|\widetilde{S}\right| \widetilde{S}_{ij}} - 4\beta \left|\overline{\widetilde{S}}\right| \overline{\widetilde{S}}_{ij}). \tag{3.9}$$

β in equation 3.9 is the ratio of the model coefficients squared at the test filter scale and at the filter scale, i.e.,

$$\beta = C_S^2(2\Delta)/C_S^2(\Delta). \tag{3.10}$$

The original (scale-invariant) dynamic model is based on the assumption that the coefficient is scale invariant and, consequently, $\beta = 1$.

Using the least squares method to minimize the error given by equation 3.8, one can obtain the optimal value of C_S^2 as

$$C_S^2 = \frac{\langle L_{ij} M_{ij} \rangle}{\langle M_{ij} M_{ij} \rangle}. \tag{3.11}$$

When implementing the dynamic model, one needs to perform some sort of averaging to ensure numerical stability. Here we use Lagrangian averaging (averaging backward over local fluid pathlines) as proposed by Meneveau et al. [49]. Only information at the previous and current time steps is stored for model coefficient calculation. This Lagrangian averaging scheme is well suited for simulations of flow over complex terrain, where the flow is non-homogeneous.

For the SGS scalar flux, the Germano identity takes the following form

$$K_i = Q_i - \bar{q}_i = \overline{\widetilde{u}_i \widetilde{\theta}} - \overline{\widetilde{u}}_i \overline{\widetilde{\theta}}, \tag{3.12}$$

where Q_i is the SGS flux at the test-filter scale $\overline{\Delta}$. Using the eddy-diffusivity model, Q_i can be calculated as

$$Q_i = -[C_S^2(\bar{\Delta}) Pr_{sgs}^{-1}] \bar{\Delta}^2 \left|\overline{\widetilde{S}}\right| \frac{\partial \overline{\widetilde{\theta}}}{\partial x_i}. \tag{3.13}$$

Combining equations 3.4, 3.12 and 3.13, one can get the error incurred by using the eddy-diffusivity model in the Germano identity for scalar transport

$$e_i = K_i - C_S^2 Pr_{sgs}^{-1}(\Delta) X_i, \tag{3.14}$$

where

$$X_i = \Delta^2 (\overline{\left|\widetilde{S}\right| \frac{\partial \widetilde{\theta}}{\partial x_i}} - 4\beta_\theta \left|\overline{\widetilde{S}}\right| \frac{\partial \overline{\widetilde{\theta}}}{\partial x_i}). \tag{3.15}$$

β_θ is a scale-dependence parameter defined as

$$\beta_\theta = C_S^2 Pr_{sgs}^{-1}(2\Delta) / C_S^2 Pr_{sgs}^{-1}(\Delta). \tag{3.16}$$

As in the case of C_S^2, the original dynamic model assumes that $C_S^2 Pr_{sgs}^{-1}$ is scale invariant and, therefore, $\beta_\theta = 1$.

Minimizing the error given by equation 3.14 using the least squares method, we get the optimal value of the lumped eddy-diffusivity coefficient as

$$C_S^2 Pr_{sgs}^{-1} = \frac{\langle K_i X_i \rangle}{\langle X_i X_i \rangle}, \tag{3.17}$$

where, in the case of the Lagrangian dynamic model, the brackets $\langle\rangle$ denote averaging along fluid pathlines.

The Lagrangian dynamic models given by equations 3.11 and 3.17 provide a systematic way to optimize the values of the coefficients C_S^2 and $C_S^2 Pr_{sgs}^{-1}$ by calculating them directly from the resolved scales in the LES. However, the standard (scale-invariant) dynamic models have been found to yield SGS dissipation rates (transfer rates of energy and scalar variance from resolved to subgrid scales) that are too small. As a result, these models produce unrealistic turbulence statistics (e.g., mean velocity and scalar profiles as well as turbulence spectra) in simulations of neutral boundary-layer flows over homogeneous [61] and heterogeneous [8, 68] flat surfaces as well as boundary layers over topography [31, 74].

3.1.3 The scale-dependent Lagrangian dynamic model

Porté-Agel et al. [61] developed a scale-dependent dynamic model. In this model, the assumption of scale invariance of the model coefficient is relaxed and the model coefficient is allowed to change with scale. Porté-Agel et al. [61] assumed that C_S^2 can be expressed as a power law function of Δ, which implies that the scale-dependence parameter β is no longer a constant value of 1 and needs to be determined dynamically. The exponent in the power-law is directly related to the value of β.

To dynamically calculate the scale-dependence parameter β, a second test filter $\widehat{\Delta}$ needs to be employed. We typically take $\widehat{\Delta} = 4\Delta$, and use a caret to denote variables filtered at scale 4Δ. The following equality is automatically satisfied once the power-law dependence of model coefficients with scale proposed by Porté-Agel et al. [61] is assumed:

$$\beta = C_S^2(4\Delta)/C_S^2(2\Delta) = C_S^2(2\Delta)/C_S^2(\Delta). \tag{3.18}$$

The error incurred by using the eddy-viscosity model in the Germano identity between scales Δ and $\widehat{\Delta}$ becomes

$$e'_{ij} = L'_{ij} - \frac{1}{3}\delta_{ij} L'_{kk} - C_S^2(\Delta) M'_{ij}, \tag{3.19}$$

where

$$L'_{ij} = \widehat{\widetilde{u}_i \widetilde{u}_j} - \widehat{\widetilde{u}}_i \widehat{\widetilde{u}}_j, \tag{3.20}$$

$$M'_{ij} = 2\Delta^2 (\widehat{\left|\widetilde{S}\right| \widetilde{S}_{ij}} - 4^2 \beta^2 \left|\widehat{\widetilde{S}}\right| \widehat{\widetilde{S}}_{ij}). \tag{3.21}$$

Minimizing the error in equation 3.19 using the earlier mentioned minimization method, we get the following equation for C_S^2:

$$C_S^2 = \frac{\langle L'_{ij} M'_{ij} \rangle}{\langle M'_{ij} M'_{ij} \rangle}. \tag{3.22}$$

Again, the brackets in equation 3.22 denote Lagrangian averaging over fluid pathlines. The scale-dependence parameter β can now be dynamically determined by combining equations 3.11 and 3.22.

For scalar fluxes, a similar scale-dependent dynamic procedure can be derived [60, 68]. In this case, the error associated with the use of the eddy-diffusivity model in the Germano identity between Δ and $\widehat{\Delta}$ becomes

$$e'_i = K'_i - C_S^2 Pr_{sgs}^{-1}(\Delta) X'_i, \tag{3.23}$$

where

$$K'_i = \widehat{\widetilde{u}_i \widetilde{\theta}} - \widehat{\widetilde{u}}_i \widehat{\widetilde{\theta}}, \tag{3.24}$$

$$X'_i = \Delta^2 (\widehat{\left|\widetilde{S}\right| \frac{\partial \tilde{\theta}}{\partial x_i}} - 4^2 \beta_\theta^2 \left|\widehat{\widetilde{S}}\right| \frac{\partial \widehat{\tilde{\theta}}}{\partial x_i}). \tag{3.25}$$

Again, the lumped model coefficient is assumed to have a power-law dependence with scale in the range of scales between the grid/filter scale and the second test filter scale so that

$$\beta_\theta = C_S^2 Pr_{sgs}^{-1}(2\Delta) / C_S^2 Pr_{sgs}^{-1}(\Delta) = C_S^2 Pr_{sgs}^{-1}(4\Delta) / C_S^2 Pr_{sgs}^{-1}(2\Delta). \tag{3.26}$$

The same method used with the first test filter is employed here to minimize the error in equation 3.23 locally backward along fluid pathlines, resulting in the following equation for $C_S^2 Pr_{sgs}^{-1}$:

$$C_S^2 Pr_{sgs}^{-1} = \frac{\langle K'_i X'_i \rangle}{\langle X'_i X'_i \rangle}. \tag{3.27}$$

Combining equations 3.27 and 3.17 results in a single equation from which the unknown scale-dependence parameter β_θ may be obtained dynamically. For more details on the scale-dependent Lagrangian dynamic procedure, see Stoll and Porté-Agel [68].

3.2 Numerical experiments

The experiment by Ross et al. [65] was carried out in the wind tunnel at the Environmental Flow Research Laboratory (EnFlo), University of Surrey, U.K. The wind tunnel has a working section of 20 m length, 3.5 m width and 1.5 m height. The fan can produce wind speed in the range between 0.3 and 4.5 m s^{-1}. A range of multi-level heaters were used to generate thermal stratification. By doing this, a maximum temperature gradient of approximately 80 K m^{-1} could be attained. To maintain a stable boundary-layer, the floor was cooled by pumping cold water through pipes beneath the floor. Roughness elements (20 mm high and 80 mm wide, separated laterally by 160 mm and downwind by 100 mm, in a triple stagger) were placed over the entire floor, including the hill surface. The velocity was measured by a two-component fibre optic, He-Ne laser Doppler anemometer with burst spectrum analysers. The free-stream velocity was measured using an ultrasonic anemometer. Measurements of temperature fluctuation were carried out using cold wires and thermocouples.

In this numerical study, the large-eddy simulation (LES) code is a modified version of the code described by Albertson and Parlange [1], Porté-Agel et al. [61], and Stoll and Porté-Agel [68]. We use pseudospectral methods to compute spatial derivatives in the horizontal directions and second order central finite differences in the vertical direction. For the entire computational domain, periodic boundary conditions are applied in the horizontal directions. Time advancement is carried out by using a second-order Adams Bashforth scheme.

A fixed stress-free lid is applied as upper boundary condition at the top of the domain. The lower boundary condition consists of using similarity theory (Monin-Obukhov similarity) to calculate the instantaneous (filtered) surface shear stress and heat flux as a function of the resolved velocity and temperature at the lowest computational level. The surface temperature is maintained at 300.5 K to match the wind tunnel conditions. In order to approximate the upstream velocity and temperature inflow boundary conditions in the wind tunnel experiment [65], we employed a relaxation zone located upwind of the hill (see Figure 3.1). The relaxation zone is set to smoothly bring the velocity and temperature fields to values corresponding to the upwind flat wind tunnel boundary layer. These velocity and temperature fields used in the relaxation zone are obtained from separate simulations over a flat surface in the absence of the hill. In these simulations, we saved the cross-sectional velocity

and temperature fields at the position corresponding to the end of the relaxation zone every 10 time steps and used them as upstream inflow boundary conditions for simulations over the two-dimensional hill. The saved velocity and temperature fields are in good agreement with the profiles measured by Ross et al. [65] without the hill. In simulations over the two-dimensional hill, we used the relaxation zone to smoothly bring the velocity and temperature fields to the saved target fields every 10 time steps. For simulations over a flat surface, a horizontal pressure gradient is exerted on the flow in the streamwise direction. The magnitude of this pressure gradient is set to match the free-stream wind speed of U =1.0 m s^{-1} measured in the wind tunnel experiments. The use of a similar relaxation zone to impose an inflow boundary condition while maintaining the accuracy of pseudospectral LES codes has been successful in previous studies of turbulent transport in urban canopies [72].

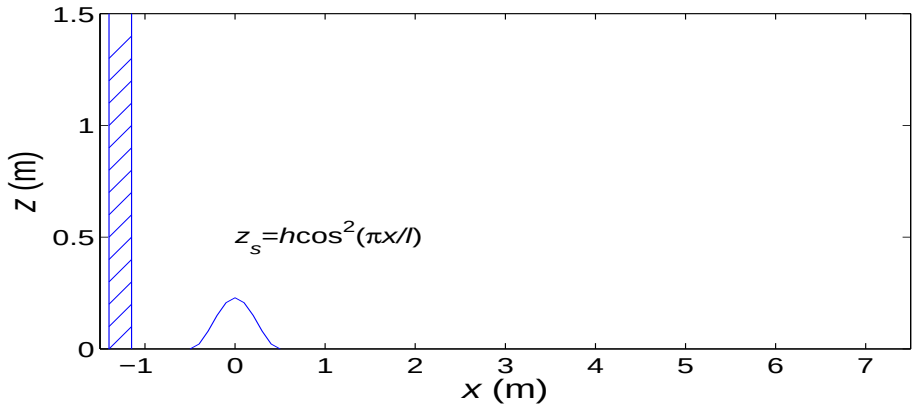

Figure 3.1: Sketch of simulation domain and relaxation zone (shaded area).

The simulated physical domain consists of the space around the two-dimensional hill with non-dimensional elevation

$$z_s/L_z = \begin{cases} (h/L_z)\cos^2(\pi x/l), & -l/2 \leq x \leq l/2 \\ 0, & \text{elsewhere} \end{cases}$$

where h/L_z is the normalized hilltop height; z_s/L_z is the normalized domain surface height; x and l are the streamwise position and width of the hill (l=1 m) respectively. The maximum slope of the hill is $\pi h/l = 0.72$, which shows the hill is steep. Figure 3.1 shows the simulation domain as well as the relaxation zone (shaded area).

The coordinate transformation developed by Clark [15] has been used to transform the physical domain into a computational domain with flat surface. It is a terrain-following transformation of the form:

$$\overline{z} = H(z - z_s)/(H - z_s), \tag{3.28}$$

where $\overline{z}$ is the vertical position in the transformed system. z is the actual elevation in the original system and H denotes the top of the domain. After the transformation, the governing equations for momentum and temperature become:

$$\begin{aligned}\frac{\partial(\sqrt{G}\widetilde{u})}{\partial t} + \sqrt{G}\widetilde{u}\frac{\partial \widetilde{u}}{\partial \overline{x}} + \sqrt{G}\widetilde{v}\frac{\partial \widetilde{u}}{\partial \overline{y}} + \sqrt{G}\widetilde{w_c}\frac{\partial \widetilde{u}}{\partial \overline{z}} + \frac{\partial(J_3\widetilde{P})}{\partial \overline{x}} + \frac{\partial(J_1\widetilde{P})}{\partial \overline{z}} \\ + \frac{\partial(J_3\tau_{11})}{\partial \overline{x}} + \frac{\partial(J_3\tau_{12})}{\partial \overline{y}} + \frac{\partial(\tau_{13} + J_1\tau_{11} + J_2\tau_{12})}{\partial \overline{z}} = 0\end{aligned} \tag{3.29a}$$

$$\begin{aligned}\frac{\partial(\sqrt{G}\widetilde{v})}{\partial t} + \sqrt{G}\widetilde{u}\frac{\partial \widetilde{v}}{\partial \overline{x}} + \sqrt{G}\widetilde{v}\frac{\partial \widetilde{v}}{\partial \overline{y}} + \sqrt{G}\widetilde{w_c}\frac{\partial \widetilde{v}}{\partial \overline{z}} + \frac{\partial(J_3\widetilde{P})}{\partial \overline{y}} + \frac{\partial(J_2\widetilde{P})}{\partial \overline{z}} \\ + \frac{\partial(J_3\tau_{12})}{\partial \overline{x}} + \frac{\partial(J_3\tau_{22})}{\partial \overline{y}} + \frac{\partial(\tau_{23} + J_1\tau_{12} + J_2\tau_{22})}{\partial \overline{z}} = 0\end{aligned} \tag{3.29b}$$

$$\begin{aligned}\frac{\partial(\sqrt{G}\widetilde{w})}{\partial t} + \sqrt{G}\widetilde{u}\frac{\partial \widetilde{w}}{\partial \overline{x}} + \sqrt{G}\widetilde{v}\frac{\partial \widetilde{w}}{\partial \overline{y}} + \sqrt{G}\widetilde{w_c}\frac{\partial \widetilde{w}}{\partial \overline{z}} + \frac{\partial \widetilde{P}}{\partial \overline{z}} + \frac{\partial(J_3\tau_{13})}{\partial \overline{x}} \\ + \frac{\partial(J_3\tau_{23})}{\partial \overline{y}} + \frac{\partial(\tau_{33} + J_1\tau_{13} + J_2\tau_{23})}{\partial \overline{z}} - \sqrt{G}g\frac{\widetilde{\theta'}}{\theta_0} = 0\end{aligned} \tag{3.29c}$$

$$\begin{aligned}\frac{\partial(\sqrt{G}\widetilde{\theta})}{\partial t} + \sqrt{G}\widetilde{u}\frac{\partial \widetilde{\theta}}{\partial \overline{x}} + \sqrt{G}\widetilde{v}\frac{\partial \widetilde{\theta}}{\partial \overline{y}} + \sqrt{G}\widetilde{w_c}\frac{\partial \widetilde{\theta}}{\partial \overline{z}} + \frac{\partial(J_3q_1)}{\partial \overline{x}} + \frac{\partial(J_3q_2)}{\partial \overline{y}} \\ + \frac{\partial(q_3 + J_1q_1 + J_2q_2)}{\partial \overline{z}} = 0,\end{aligned} \tag{3.29d}$$

where $\overline{x}$, $\overline{y}$, $\overline{z}$ are the curvilinear coordinates in the computational domain, $\widetilde{u}$, $\widetilde{v}$, $\widetilde{w}$ are filtered velocities in the physical domain, $\widetilde{w_c}$ denotes the filtered vertical velocity in the computational domain, $\widetilde{\theta}$ is the filtered temperature, $\widetilde{P}$ represents the filtered pressure, $\sqrt{G}$ is the determinant of the Jacobian matrix of transformation, J_1, J_2, J_3 are non-zero components of the Jacobian matrix of transformation, τ_{11}, τ_{12}, τ_{13}, τ_{22}, τ_{23}, τ_{33} are the subgrid-scale (SGS) stresses, q_1, q_2, q_3 denote SGS heat fluxes, g is the gravitational acceleration, $\widetilde{\theta_0}$ is a reference temperature, $\widetilde{\theta'}$ is the fluctuation of the filtered temperature. Taking the divergence of the discretized momentum

equations and applying the continuity equation, we can obtain the pressure Poisson equation. The pressure Poisson equation is solved iteratively at every time step until the solution is converged. The computational domain is of size 9 m×1.5 m×1.5 m, that is $(2\pi, \pi/3, \pi/3)$ in non-dimensionalized form by using a length scale of L_z=1.432 m. The normalized effective surface roughness is $z_0/L_z = 1.606 \times 10^{-3}$. The computational domain is divided into $180 \times 30 \times 120$ uniformly spaced grid points. The grid is staggered in the vertical direction, with the vertical velocity stored halfway between the other variables. The relaxation zone covers 6 grid points in the streamwise direction. A sponge layer is applied at the domain top to absorb possible gravity waves. The time step used in the simulations is 0.002864 s, and the duration of the simulation is 429 s.

The temperature field of this stably-stratified boundary-layer flow is composed of two layers with different levels of stratification: a region of relatively weak stratification of about 10 K m^{-1} in the lowest 0.5 m, and a region of stronger stratification (about 40 K m^{-1}) above (z >0.5 m). The simulations are run for a period of time long enough to guarantee quasi-steady flow conditions and statistical convergence of the results presented in the next section.

3.3 Results

Figure 3.2 (a) shows a contour plot of the streamwise velocity u (in m s^{-1}) measured during the wind tunnel experiment in a vertical plane perpendicular to the two-dimensional hill [65]. Figures 3.2 (b) to 3.2 (d) show similar contour plots of averaged (in time and spanwise direction) streamwise velocities simulated using large-eddy simulation (LES) with different subgrid-scale (SGS) models: the Smagorinsky model (Figure 3.2 (b)), the Lagrangian dynamic model (Figure 3.2 (c)), and the scale-dependent Lagrangian dynamic model (Figure 3.2 (d)). Comparison of Figure 3.2 (a) and Figure 3.2 (b) reveals important differences between the measured velocity field and the simulated velocity obtained with the Smagorinsky model. In particular, the Smagorinsky model grossly overpredicts the size of the recirculation region on the lee side of the hill. The location of the separation point predicted by the Smagorinsky model is around the hill top. Moreover, the model underpredicts the velocity magnitude right above the hill top.

Figure 3.2 (c) and Figure 3.2 (d) show that both dynamic models improve the

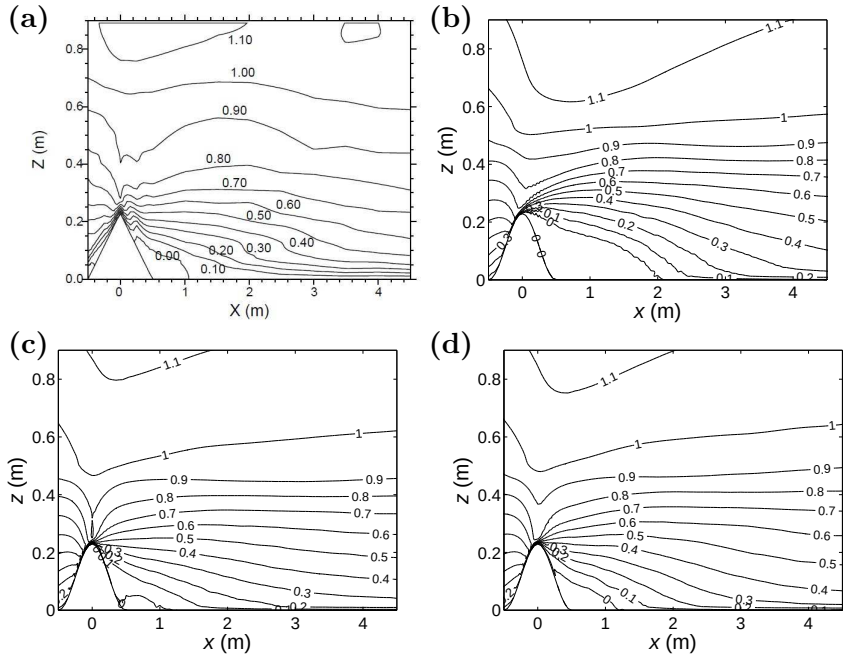

Figure 3.2: Contour plots of streamwise velocity u (in m s^{-1}) in a vertical plane perpendicular to the hill: (a) Wind-tunnel measurements (Ross et al. 2004), (b) Smagorinsky model, (c) Lagrangian dynamic model, (d) scale-dependent Lagrangian dynamic model.

velocity prediction with respect to the Smagorinsky model. The Lagrangian dynamic model, however, is found to underestimate the size of the recirculation region. From Figure 3.2 (c), we can see that the separation point is near the downwind foot of the hill. Moreover, this model overestimates the magnitude of the streamwise velocity right above the hill crest. A similar velocity overestimation from the Lagrangian dynamic model was reported in numerical simulations of neutral turbulent flows over two-dimensional topography [31, 74]. Overall, the scale-dependent Lagrangian dynamic model provides a more accurate prediction of the streamwise velocity field (Figure 3.2 (d)), compared with the Smagorinsky model and the scale-invariant dynamic model. In particular, the recirculation region predicted by the scale-dependent dynamic model matches more closely the one measured in the wind tunnel experiment (Figure 3.2 (a)). The separation point is about halfway downwind from the hill crest.

Figure 3.3 (a) shows the contour plot of momentum flux $\overline{u'w'}$ (in m^2 s^{-2}) measured during the wind tunnel experiment in a vertical plane perpendicular to the two-dimensional hill [65]. Figures 3.3 (b) to 3.3 (d) show similar contour plots of

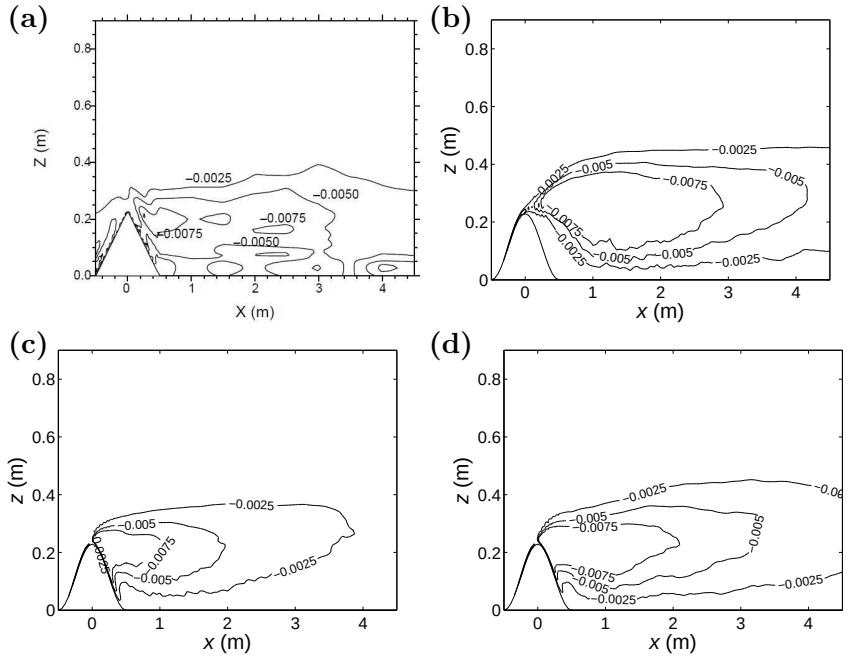

Figure 3.3: Contour plots of momentum flux $\overline{u'w'}$ (in m^2 s^{-2}) in a vertical plane perpendicular to the hill: (a) Wind-tunnel measurements (Ross et al. 2004), (b) Smagorinsky model, (c) Lagrangian dynamic model, (d) scale-dependent Lagrangian dynamic model.

time-averaged momentum flux $\overline{u'w'}$ (resolved stress plus subgrid-scale stress) simulated using LES with different SGS models: the Smagorinsky model (Figure 3.3 (b)), the Lagrangian dynamic model (Figure 3.3 (c)), and the scale-dependent Lagrangian dynamic model (Figure 3.3 (d)). From these figures, we can see that, because of the very strong stratification (about 40 K m^{-1}) in the upper part of the domain (above 0.5 m), turbulence was largely confined in the lower part of the domain. By comparing the contour line of value -0.005 m^2 s^{-2} in Figure 3.3 (a) and Figure 3.3 (b), the Smagorinsky model (Figure 3.3 (b)) is found to somewhat overestimate the size of the wake region downwind of the hill, which leads to larger prediction of $\overline{u'w'}$ values in the domain. The Lagrangian dynamic model clearly underpredicts the size of the wake region behind the hill. Note that in Figure 3.3 (c) the region with magnitude of flux values above 0.005 m^2 s^{-2} is much smaller than the region obtained from wind tunnel measurements (Figure 3.3 (a)) and from the scale-dependent Lagrangian dynamic model (Figure 3.3 (d)). The scale-dependent Lagrangian dynamic model gives a more accurate prediction of the wake region behind the hill.

The dynamically calculated values of the eddy-viscosity model coefficient C_S^2

obtained using the Lagrangian dynamic and scale-dependent Lagrangian dynamic models are presented in Figures 3.4 (a) and 3.4 (b), respectively. The values represent averages in the spanwise direction and in time. In the upper portion of the domain, both models yield relatively low values of C_S^2 due to the very strong flow stratification in that region. This is consistent with previous studies that show C_S^2 decreases with increasing stability [39, 38, 62]. The coefficients obtained with both dynamic models decrease near the surface to account for the reduction in the characteristic scales of the turbulence in that region of the flow. In addition, strong variability of the dynamically calculated C_S^2 is found around the crest of the hill, where the flow is heterogeneous in both the streamwise and vertical directions. Smaller values of C_S^2 are obtained over the upwind side of the hill crest, where the flow undergoes strong straining; larger C_S^2 values are found in the downhill side of the hill, where the flow detaches from the surface, recirculates and experiences much smaller straining.

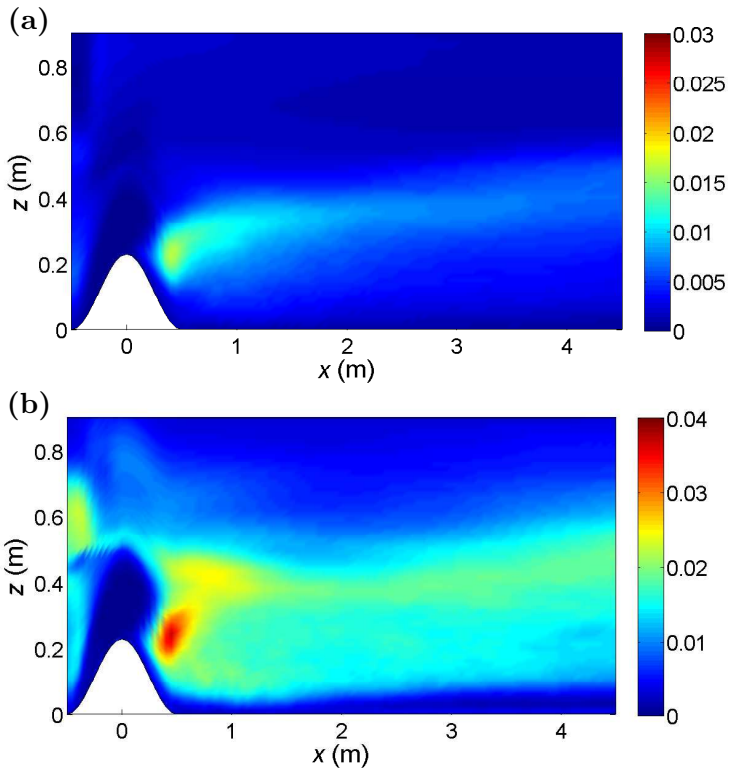

Figure 3.4: Smagorinsky coefficient C_S^2 calculated dynamically with: (a) the Lagrangian dynamic model, (b) the scale-dependent Lagrangian dynamic model.

The values of the eddy-diffusivity model coefficient $C_S^2 Pr_{sgs}^{-1}$ obtained using the

Lagrangian dynamic and scale-dependent Lagrangian dynamic model are presented in Figures 3.5 (a) and 3.5 (b), respectively. The values represent averages in the spanwise direction and in time. Similar to C_S^2, the value of the lumped coefficient $C_S^2 Pr_{sgs}^{-1}$ is small in the upper part of the domain to account for the reduction in the characteristic scale of the turbulence associated with the strong stratification of the flow [39, 38, 62]. In the lower part, $C_S^2 Pr_{sgs}^{-1}$ is found to decrease as the surface is approached in order to account for the reduction in the characteristic scale of the turbulence near the surface. Horizontal variation of the lumped coefficient $C_S^2 Pr_{sgs}^{-1}$ is also manifest in the figures.

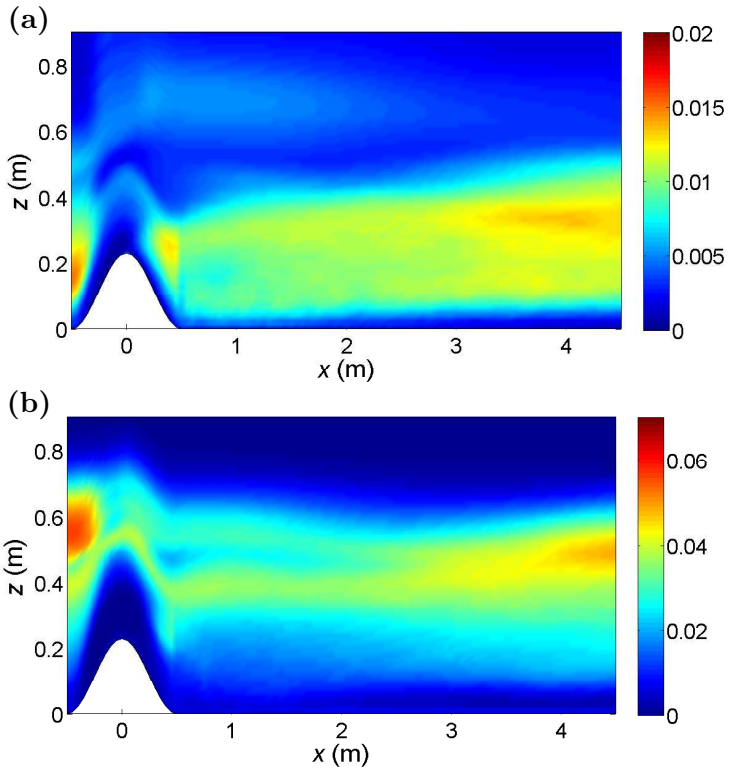

Figure 3.5: Lumped eddy-diffusivity coefficient $C_S^2 Pr_{sgs}^{-1}$ calculated dynamically with: (a) the Lagrangian dynamic model, (b) the scale-dependent Lagrangian dynamic model.

Figures 3.6 (a) and 3.6 (b) show the scale-dependence parameters β ($= C_S^2(2\Delta)/C_S^2(\Delta)$) and β_θ ($= C_S^2 Pr_{sgs}^{-1}(2\Delta)/C_S^2 Pr_{sgs}^{-1}(\Delta)$) obtained with the scale-dependent Lagrangian dynamic models. As expected, the scale-dependence parameters become smaller as the surface is approached due to increased shear and anisotropy of the flow. The smallest values of β and β_θ are found near the upwind side of the hill

crest, where the mean shear and anisotropy of the flow are stronger; downwind of the hill, where the flow separates and becomes more isotropic, the scale-dependence coefficients are larger. These overall trends are consistent with the results obtained for β in simulations of a neutral boundary layer over a sinusoidal surface [74].

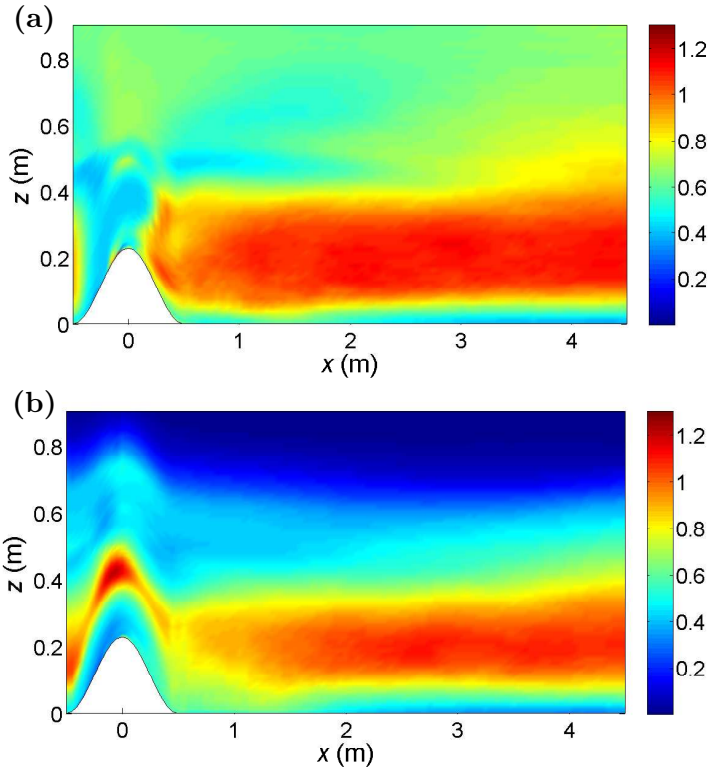

Figure 3.6: Scale-dependence parameters β (a) and β_θ (b) obtained with the scale-dependent Lagrangian dynamic model.

Figures 3.7 (a) to 3.7 (c) show contour plots of averaged (in time and spanwise direction) resolved turbulent kinetic energy (in $m^2\ s^{-2}$) obtained with the three SGS models under consideration. On the upwind side of the hill crest, the Lagrangian dynamic model predicts the largest kinetic energy among the three models, while the Smagorinsky model yields the smallest. This is in agreement with previous studies (e.g., [61]) which show that the Lagrangian dynamic model is not dissipative enough in the near-ground region, yielding too much resolved kinetic energy. In contrast, the Smagorinsky model is known to be too dissipative near the ground. The scale-dependent dynamic model has been found to provide more realistic SGS dissipation rates in simulations of flat homogeneous boundary layers (e.g., [61]). In the downwind wake region, away from the hill, the magnitude of turbulent kinetic

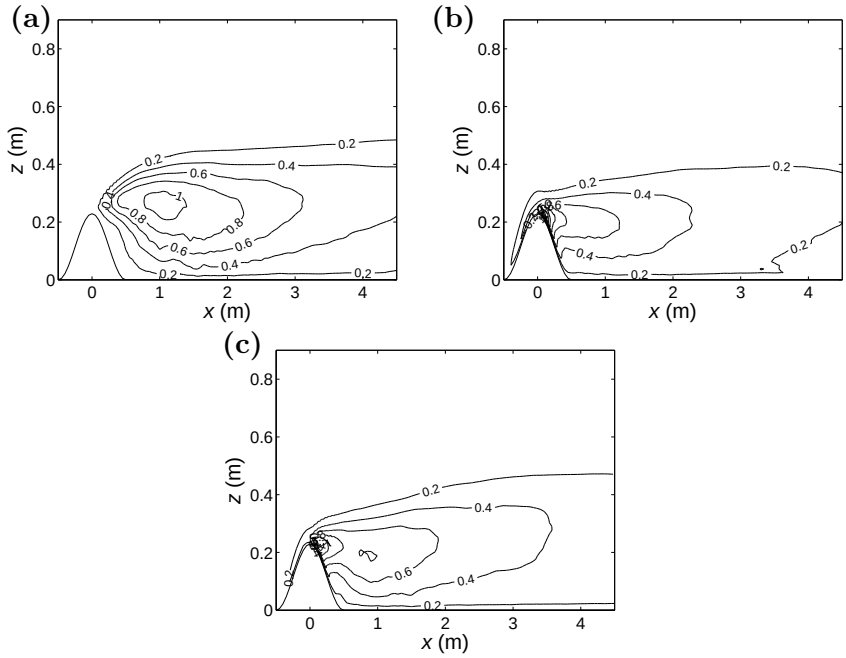

Figure 3.7: Contour plots of resolved turbulent kinetic energy (in $m^2\ s^{-2}$) in a vertical plane perpendicular to the hill: (a) Smagorinsky model, (b) Lagrangian dynamic model, (c) scale-dependent Lagrangian dynamic model.

energy obtained with the Lagrangian dynamic model is clearly smaller than that obtained with the Smagorinsky model and the scale-dependent Lagrangian dynamic model. The Smagorinsky model yields the greatest turbulent kinetic energy among the three models. This is in accordance with findings from previous studies (e.g., [31, 53]), which reported that the standard Smagorinsky model overestimates the turbulent kinetic energy in the free shear layer behind the obstacle. The differences in the prediction of the resolved turbulent kinetic energy in the wake region, and the size of that region can be explained in part by the differences in the simulated flow on the upwind side of the hill crest. In order to better understand that effect, contour plots of the averaged (in time and spanwise direction) vertical velocity component are shown in Figure 3.8 for the three models under consideration. From that figure, it is clear that the Smagorinsky model leads to a relatively large prediction of the vertical velocity over the upwind side of the hill crest (Figure 3.8 (a)). This is consistent with the underestimation of the streamwise velocity in that region (Figure 3.2 (b)), and leads to an excessive upward deflection of the flow. This, in turn, leads to large resolved kinetic energy in the downstream region of the hill (Figure 3.7

(a)) and the formation of unrealistically large wake and recirculation regions there. This effect is also reflected in the contour lines of mean temperature predicted with the Smagorinsky model (Figure 3.9 (a)), which show a stronger upward deflection compared with the ones obtained with the two dynamic models. In contrast, the Lagrangian dynamic model predicts a relatively larger horizontal velocity (Figure 3.2 (c)) and smaller vertical velocity (Figure 3.8 (b)) on the upwind side of the hill crest, which produces a smaller upward deflection of the flow. This translates into smaller vertical mixing, resolved kinetic energy (Figure 3.7 (b)) and wake size in the downwind region of the hill. This is also consistent with the contours of temperature, which show smaller upward deflection around the hill (Figure 3.9 (b)), compared with the Smagorinsky model (Figure 3.9 (a)).

It is important to point out that our results near the upwind side of the hill crest agree with previous studies that found that the scale-dependent dynamic model has better SGS dissipation characteristics in the surface layer, compared with the Smagorinsky and scale-invariant dynamic models. Near the surface, those models are too dissipative and not dissipative enough, respectively (e.g., [8, 61, 69, 74]). In general, the results presented here also agree with previous studies that found the scale-dependent dynamic model yields improved predictions of the
flow statistics (e.g., average velocity and turbulent fluxes), not only in the surface layer, but throughout most of the computational domain.

3.4 Summary

Large-eddy simulation (LES) has been used to investigate stably-stratified turbulent boundary-layer flow over a steep two-dimensional hill. Three different types of subgrid-scale (SGS) models for both the SGS stresses and SGS heat fluxes are tested: (a) the Smagorinsky model, (b) the Lagrangian dynamic model, and (c) the scale-dependent Lagrangian dynamic model [68]. Simulation results obtained with the different models are compared with turbulence statistics obtained from experiments conducted in the environmental wind tunnel at the Environmental Flow Research Laboratory (EnFlo), University of Surrey in the U.K. [65].

In this stably-stratified turbulent boundary-layer flow simulation, the standard (non-dynamic) Smagorinsky model yields relatively poor predictions of the turbulent statistics, arguably due to its failure to adjust the model coefficients to capture the spatial variations of the length scales in the SGS eddy viscosity and eddy diffusivity.

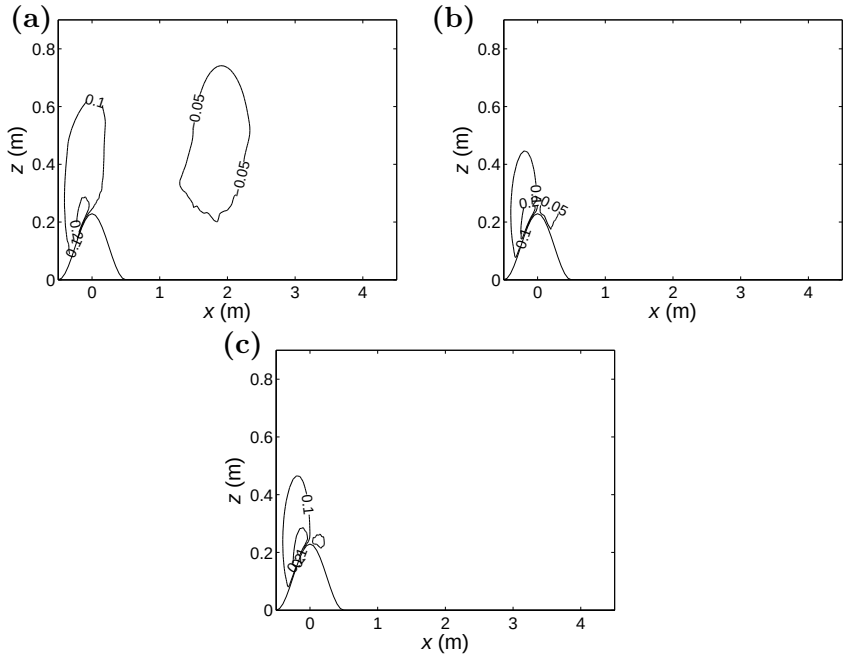

Figure 3.8: Contour plots of vertical velocity w (in m s^{-1}) in a vertical plane perpendicular to the hill: (a) Smagorinsky model, (b) Lagrangian dynamic model, (c) scale-dependent Lagrangian dynamic model.

In particular, this model is found to be too dissipative near the surface on the upwind side of the hill crest, and to overpredict the upward deflection of the flow in that region. This is consistent with previous studies of neutral boundary-layer flow over topography [74], and it is associated with an overprediction of the size of the simulated wake region.

Dynamic models offer a more systematic way of optimizing the local value of the eddy viscosity and eddy diffusvity SGS model coefficients by computing them dynamically at every time step and position in the flow based on the dynamics of the smallest resolved scales (between the grid/filter scale and a test filter scale). As a result, both the Lagrangian dynamic model and the scale-dependent Lagrangian dynamic model show improved predictions with respect to the standard non-dynamic models. However, the Lagrangian dynamic model is not dissipative enough and overestimates the horizontal velocity above the hill crest. This is consistent with the results from previous LES studies of neutral boundary-layer flow over two-dimensional hills [31, 74]. This model is found to underpredict the size of the downwind wake region.

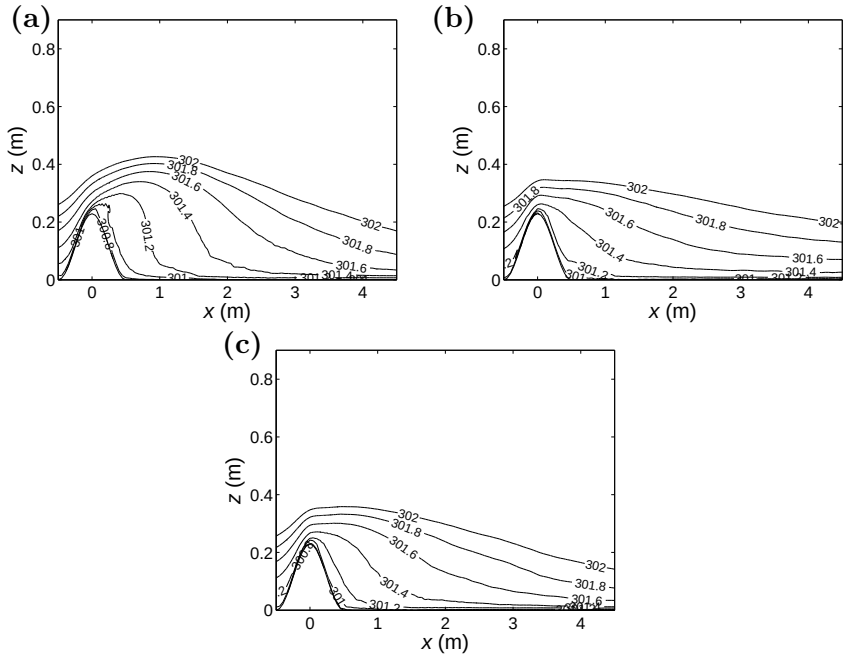

Figure 3.9: Contour plots of temperature θ (in K) in a vertical plane perpendicular to the hill: (a) Smagorinsky model, (b) Lagrangian dynamic model, (c) scale-dependent Lagrangian dynamic model.

By relaxing the assumption of scale invariance in the dynamic model, the scale-dependent dynamic model [61, 68] is able to dynamically (without any parameter tuning) capture the scale dependence of the model coefficient associated with regions of the flow with strong shear and/or thermal stratification. Our results show that this procedure substantially improves the simulation results with respect to both the standard (non-dynamic) eddy-viscosity/diffusivity model and the scale-invariant dynamic model.

Chapter 4

A large-eddy simulation study of turbulent flow over multiscale topography

Abstract

Most natural landscapes are characterized by multiscale (often multifractal) topography with well-known scale-invariance properties. For example, the spectral density of landscape elevation fields is often found to have a power-law scaling behaviour (with a -2 slope on a log-log scale) over a wide span of spatial scales, typically ranging from tens of kilometres down to a few metres. Even though the effect of topography on the atmospheric boundary layer (ABL) has been the subject of numerous studies, few have focussed on multiscale topography. In this study, large-eddy simulation (LES) is used to investigate boundary-layer flow over multiscale topography, and guide the development of parametrizations needed to represent the effects of subgrid-scale (SGS) topography in numerical models of ABL flow. Particular emphasis is placed on the formulation of an effective roughness used to account for the increased aerodynamic roughness associated with SGS topography. The LES code uses the scale-dependent Lagrangian dynamic SGS model for the turbulent stresses and a terrain-following coordinate transformation to explicitly resolve the effects of the topography at scales larger than the LES resolution. The terrain used in the simulations is generated using a restricted solid-on-solid (RSOS) landscape evolution model, and it is characterized by a -2 slope of the elevation power spectrum. Results from simulations performed using elevation fields pass-filtered at different spatial resolutions indicate a clear linear relation between the square of the effective roughness and the variance of elevation.

4.1 Introduction

The interaction between natural forces (e.g., geological uplift, overland water flow and erosion) and the earth's surface results in various geomorphic processes that shape landscapes at a wide range of spatial and temporal scales. As a result, natural landscapes exhibit multiscale (often multifractal) structure, a high degree of self-similarity, and well-known scaling properties (e.g., [64]). For example, the power spectra of linear transects in many natural landscapes, when plotted on a log-log scale, show a clear -2 slope over a wide range of spatial scales, from a few metres up to tens of kilometres (e.g., [29, 56]). Undoubtedly, the scaling properties of surface elevation have effects on the multiscale properties of turbulent atmospheric boundary-layer (ABL) flows, and the corresponding surface fluxes of momentum and scalars.

The interaction between the ABL and topography has been the focus of numerous previous studies (e.g., [46, 41,79, 77, 11]). The drag force that landscapes exert on the ABL attracts particular attention (e.g., [79]) because of its significant influence on the ABL flow and turbulent fluxes, which need to be parametrized in atmospheric numerical models. For ABL flow over topography, the drag force consists of both surface friction drag and form drag induced by the topography. There are several ways to account for the overall effect of both types of drag on the flow. These include the bulk similarity approach, consisting of using an effective aerodynamic roughness length within the framework of Monin-Obukhov similarity theory (e.g., [26, 79, 50, 11]), and the orographic stress approach [78]. The effective aerodynamic roughness length approach is the most commonly used. For natural landscapes, due to their multiscale properties, it is reasonable to expect that the effective aerodynamic roughness should depend on the numerical model grid resolution. This potential scale-dependence of the effective aerodynamic roughness should be taken into account in relatively high-resolution models, for which the grid resolution falls within the power-law scaling range of the topography.

Several field studies have been carried out to determine the effective roughness length of natural landscapes (e.g., [41, 19]). In these studies, the effective roughness is obtained by applying bulk similarity theory to vertical wind-profile data collected using radiosondes (e.g., [41]) or meteorological towers (e.g., [19]). Another way to estimate the effective roughness length of natural landscapes from field measurements is to collect land-surface information via airborne laser altimetry (e.g., [19])

and apply parametrization schemes (e.g., [41, 26]) based on surface geometrical parameters such as the frontal or silhouette area of the hills and the base area of the hills.

Most large-eddy simulation (LES) studies of flow over topography have been restricted to flows over simple topographies consisting of two- or three-dimensional idealized shapes (e.g., [79, 6, 11, 20, 31, 74, 75]). Several of those studies have used simulation results to determine the effective roughness length of the simple topographies (e.g., [79, 6, 11]). However, LES has yet to be used to study flow over explicitly-resolved multi-scale topography and to investigate the scaling properties of the corresponding effective surface aerodynamic roughness for different grid resolutions.

In this paper, LES is used to study the effect of multi-scale subgrid-scale (SGS) topography on the overall SGS drag exerted by landscapes on the ABL. It is important to note here that the term SGS refers to quantities that are associated with scales smaller than the grid resolution in other numerical models (different from the LES used in this study) that have coarser resolution (e.g., coarser LES models or high-resolution weather forecast models). In particular, the LES results are used to investigate how the effective roughness length relates to surface information such as the subgrid-scale variance of surface elevation. To achieve that, a landscape evolution model, the so-called restricted solid-on-solid (RSOS) model [37], is used to generate a periodic multi-scale topography with statistical properties (e.g., the power spectrum of the elevation field) similar to those of natural landscapes. LES models with the tuning-free scale-dependent Lagrangian dynamic subgrid model [68] are performed to simulate ABL flow over multiscale landscapes, and the results used to study the behaviour of the corresponding effective roughness length. Next, brief summaries of the LES technique and the RSOS landscape model are provided.

4.1.1 Large-eddy simulation

Large-eddy simulation has been widely used to study the effect of topography on turbulent transport in boundary-layer flow (e.g., [40, 73, 27, 10, 31, 74, 75]). LES solves the Navier-Stokes equations that have been filtered using a three-dimensional spatial filter. As a result, LES explicitly resolves all the turbulent flow scales larger than the filter size, and parametrizes smaller scales using a subfilter-scale (SFS)

model. The filtered Navier-Stokes equations, written in rotational form, are:

$$\frac{\partial \widetilde{u}_i}{\partial t} + \widetilde{u}_j(\frac{\partial \widetilde{u}_i}{\partial x_j} - \frac{\partial \widetilde{u}_j}{\partial x_i}) = -\frac{1}{\rho}\frac{\partial \widetilde{p}^*}{\partial x_i} - \frac{\partial \tau_{ij}}{\partial x_j} + F_i, \tag{4.1}$$

where $\widetilde{u}_i$ is the filtered velocity in the i direction, $\widetilde{p}^* = \widetilde{p} + \frac{1}{2}\rho\widetilde{u}_j\widetilde{u}_j$ is the modified pressure, $\widetilde{p}$ is the filtered pressure, ρ is the air density, τ_{ij} is the SFS stress tensor, and F_i is a forcing term (e.g., a mean pressure gradient in the streamwise direction). The SFS stresses τ_{ij} are parametrized using a SFS model.

An eddy-viscosity model is often used to parametrize the deviatoric part of the SFS stress as follows [67]:

$$\tau_{ij} - \frac{1}{3}\delta_{ij}\tau_{kk} = -2\nu_{sgs}\widetilde{S}_{ij}, \tag{4.2}$$

$$\nu_sgs = [C_S\Delta]^2 \left|\widetilde{S}\right|, \tag{4.3}$$

where $\widetilde{S}_{ij} = \frac{1}{2}\left(\frac{\partial \widetilde{u}_i}{\partial x_j} + \frac{\partial \widetilde{u}_j}{\partial x_i}\right)$ is the resolved strain-rate tensor, ν_{sgs} is the eddy viscosity, the strain-rate tensor magnitude is calculated as $\left|\widetilde{S}\right| = \left(2\widetilde{S}_{ij}\widetilde{S}_{ij}\right)^{\frac{1}{2}}$, Δ is the size of the spatial filter, and C_S is the Smagorinsky coefficient.

One of the main challenges in the implementation of the Smagorinsky model is the specification of the model coefficient. The value of C_S is well established for isotropic turbulence. In that case, if a cut-off filter is used in the inertial subrange and the filter scale Δ is equal to the grid size, then $C_S \approx 0.17$ [42]. However, anisotropy of the flow, particularly the presence of a strong mean shear near the surface and around topography in high-Reynolds-number ABL flows, makes the optimum value of C_S depart from its isotropic counterpart (e.g., [68, 74, 75]).

To avoid the need for a priori specification or tuning of the model coefficient, Germano et al. [23] proposed the so-called dynamic procedure, which calculates the value of the model coefficient at every time and position in the flow based on information from the smallest resolved scales. In particular, it minimizes the error incurred when using the Smagorinsky model to compute the resolved Leonard stress (defined using a test filter scale $\bar{\Delta}$, typically of size 2Δ) while assuming scale invariance of the coefficient in that range of scales. However, recent studies have shown that the assumption of scale invariance in the dynamic model can lead to errors in simulated boundary-layer flows over both flat surfaces [61] as well as complex terrain [31, 74, 75].

By relaxing the assumption of scale invariance in the dynamic model, Porté-Agel et al. [61] proposed the scale-dependent dynamic model. In this model, two test filters of size $\bar{\Delta}$ (typically 2Δ) and $\widehat{\Delta}$ (typically 4Δ) are introduced and used in the dynamic procedure, together with the assumption that the model coefficient has a power-law dependence with scale. When implementing the scale-dependent dynamic model, one needs to use some kind of averaging to guarantee numerical stability. Stoll and Porté-Agel [68] proposed the Lagrangian scale-dependent dynamic model, which employs Lagrangian averaging [49]. Lagrangian averaging consists of averaging over flow pathlines, which makes this model particularly suitable for simulations of non-homogeneous flows. Further details about the Lagrangian scale-dependent dynamic model can be found in Stoll and Porté-Agel [68].

The performance of the Lagrangian scale-dependent dynamic model has been assessed and compared with that of other commonly used SGS models in simulations of neutral [74] as well as stably-stratified [75] boundary-layer flow over simple sinusoidal hills. By comparing simulation results with wind-tunnel data, these studies showed that the Lagrangian scale-dependent dynamic model, which allows for scale dependence of the eddy-viscosity and eddy-diffusivity model coefficients associated with flow anisotropy, predicts more accurate turbulence statistics than the standard Smagorinsky model and Lagrangian (scale-invariant) dynamic model. For this reason, the Lagrangian scale-dependent dynamic model [68] is employed in this study to parametrize SFS stresses in neutral boundary-layer flow over multiscale topography.

4.1.2 Landscape modelling

In order to perform large-eddy simulations of ABL flow over multiscale topography using periodic boundary conditions compatible with the pseudospectral numerical methods used by many LES models, it is desirable to use surface elevation fields that are periodic. To achieve that, here we generate synthetic periodic multiscale complex terrain using a landscape evolution model, the restricted solid-on-solid (RSOS) model. This model was proposed by Kim and Kosterlitz [37], and it was initially used to simulate the growth of surface interfaces. Park and Kahng [55] derived the continuous Kardar-Parisi-Zhang (KPZ) equation [35] from the RSOS model, and proved they are the same in the continuum limit. Both the KPZ equation and the RSOS model have been used extensively to simulate landscape evolution and surface

growth (e.g., [36, 58]).

In the RSOS procedure proposed by Kim and Kosterlitz [37], the surface elevation of a two-dimensional lattice of points is updated by random deposition by using the following rules: the elevation of the point is increased by one if the elevation at this point is smaller than or equal to the elevation of all of its four nearest neighbouring points; however, if this criterion is not satisfied, the elevation of the point remains unchanged. This rule ensures that the elevation difference between any point and its nearest four neighbouring points can only take the value of -1, 0 or 1, which prevents the formation of overhangs or vacancies. This random deposition process is repeated until a steady-state condition is attained for which the surface height is equal to or greater than the linear dimension of the lattice.

The elevation power spectra of the surfaces generated with the RSOS model show a power-law dependence on wavenumber with exponent close to -2 over a wide range of scales. This makes the surface a good approximation to natural landscapes (e.g., [29]). An important advantage of the RSOS model, compared to other synthetic topography generation models that assume a Gaussian probability distribution function (PDF) of topography, is that it is able to produce topographies that have more realistic PDFs. The topography of the earth's surface is skewed in a way such that a much larger percentage of the total landscape is represented by lowlands (topography with an elevation smaller than the median elevation for a region) than highlands. The RSOS model is able to capture this skewness characteristic of the PDF of the elevation of natural landscapes, thus yielding more realistic elevation fields compared with Gaussian models, which are only able to produce a non-skewed Gaussian PDF of elevation (e.g., [76, 57]).

To understand the effect of multi-scale topography on subgrid-scale drag forces that require parametrization in high-resolution numerical models (e.g., weather forecast models or LES), it is of interest to study the relationship between effective aerodynamic roughness and subgrid-scale landscape characteristics. In particular, the aerodynamic roughness is expected to increase with increasing SGS variance of the elevation field (variance of surface elevation associated with the SGS topography). The SGS variance of the elevation field is defined as:

$$\sigma^2_{h,sgs} = \langle \widehat{hh} - \widehat{h}\widehat{h} \rangle, \tag{4.4}$$

where h is the surface elevation, the hat symbol and $\langle \ \ \rangle$ denote spatial filtering at a resolution of the numerical model (Δ_{model}) and area averaging, respectively. Note

that, in the case of zero SGS variance (no SGS topography), the effective roughness is equal to the aerodynamic roughness of the surface. Besides this limiting behaviour, the functional relationship between effective roughness and SGS variance of elevation is not known. As a first-order approximation, one could assume a linear relation between the effective roughness and the variance of the elevation field (e.g., [80, 22, 2]). Further more, in order to comply with the above-mentioned lower limit for the aerodynamic roughness, here we propose to use:

$$(z_o^{eff})^2 - z_o^2 = C\sigma_{h,sgs}^2 = C\langle \widehat{hh} - \widehat{h}\widehat{h} \rangle, \tag{4.5}$$

where C is a proportionality factor, assumed to be constant for a given landscape (topography and aerodynamic roughness combination).

In our study, large-eddy simulations using the scale-dependent Lagrangian dynamic model are performed of ABL flows over a series of multiscale complex topographies. The simulation results are used to examine the relation between SGS variance of elevation $\sigma_{h,sgs}^2$ and effective roughness length associated with the SGS topography. Particular emphasis is placed on evaluating the linear model given by equation 4.5. Simulation details are explained in the following section.

4.2 Numerical experiments

A detailed description of the LES code used in this numerical study can be found in Albertson and Parlange [1], Porté-Agel et al. [61], Stoll and Porté-Agel [68] and Wan et al. [74]. The spatial derivatives are computed using pseudospectral methods in the horizontal directions with periodic boundary conditions, and finite differences in the vertical direction. The lower boundary condition applies similarity theory (the surface-layer logarithmic law) to calculate the instantaneous (filtered) surface shear stress based on the velocity field at the lowest computational level. The upper boundary condition is a fixed stress-free lid, while time advancement is realized through the second-order Adams-Bashforth scheme.

The lower surface of the physical domain consists of a series of periodic multiscale topographies obtained by spatially filtering a multiscale terrain generated using the restricted solid-on-solid (RSOS) model [37]. These terrains approximate (statistically) SGS topography of natural landscapes. The RSOS model is applied here starting from a flat initial surface of zero elevation, and discretizing it as a lattice with 96×96 uniformly distributed grid points. Periodic boundary conditions

are enforced in both horizontal directions. The RSOS procedure described above is applied 8×10^6 times to obtain a multiscale complex terrain (not shown here). The simulated terrain is periodic in both x and y directions, and is then shifted to a mean height of zero and scaled in all three directions to fit the LES domain dimensions, which have non-dimensional values of 2π, 2π and 2. A surface T_0 (shown in Figure 4.1) is therefore obtained. The elevation power spectral density of terrain T_0 is plotted against wavenumber in a log-log scale in Figure 4.2. The spectral density of elevation shows a clear -1.8 slope, which is very close to the -2 slope of the elevation power spectrum reported for natural topography (e.g., [29]); this feature makes the obtained terrain a reasonable approximation to natural landscapes for the purpose of studying the effect of multiscale topography on ABL flow.

Starting from the RSOS-simulated multiscale terrain shown in Figure 4.1, we generate a series of multiscale complex terrains containing different ranges of scales in the elevation power spectrum. This is achieved by means of two-dimensional band-pass spatial filtering. The resulting landscapes can be considered to be SGS topography in larger-scale models (e.g., LES or weather forecast models) of different spatial resolutions. In order to guarantee that the effects of all scales existing in the considered terrains are properly captured by the LES, first we apply a low-pass filter at scale $4\sqrt{2}\Delta$ (about six times the LES grid size Δ). This filtering operation retains only the terrain fluctuations of horizontal size larger than that scale. Therefore, that scale can be considered as the smallest size of topographic features that can be identified in the simulated terrain (corresponding to the scale below which hill-slope diffusion processes dominate during landscape evolution). Furthermore, in order to simulate the effect of different ranges of scales (SGS in larger-scale models), we apply a second high-pass filter at different scales: $4\sqrt{2}\Delta$, 8Δ, $8\sqrt{2}\Delta$, 16Δ, $16\sqrt{2}\Delta$, and $32\sqrt{2}\Delta$, respectively, and obtain six filtered terrains. It is important to point out that, at scale $32\sqrt{2}\Delta$, the filtered terrain contains all the large scales of the original RSOS terrain. Considering elevation fields between scale $4\sqrt{2}\Delta$ and 8Δ, $4\sqrt{2}\Delta$ and $8\sqrt{2}\Delta$, $4\sqrt{2}\Delta$ and 16Δ, $4\sqrt{2}\Delta$ and $16\sqrt{2}\Delta$, $4\sqrt{2}\Delta$ and $32\sqrt{2}\Delta$, we obtain a series of SGS terrains: T_1, T_2, T_3, T_4, T_5 (shown in Figure 4.3). From Figure 4.3, it is clear that, as the scale increases, the magnitude of terrain elevation increases, and larger-size topographic structures are included in the terrains. The statistics of the SGS terrains considered here are shown in Table 1. As expected, the inclusion of more (larger) scales in the terrains from T_1 to T_5 leads to an increase in the level of surface variability, which results in increasing SGS variance of elevation.

The LES models uses the terrain-following coordinate transformation developed by Clark [15]. It is used to transform the physical domains containing the multi-scale topographies T_1 to T_5 into a flat computational domain by using the following equation:

$$\overline{z} = H(\frac{z - z_s(x,y)}{H - z_s(x,y)}), \tag{4.6}$$

where $\overline{z}$ is the vertical position in the transformed system, z represents distance to the complex surface in the original system, z_s and H denote the actual elevation (in the original system) of the terrain and the top of the domain, respectively.

The dimensions of the computational domain are 2π, 2π and 2 in the streamwise, spanwise and vertical directions, respectively, after being normalized with a length scale of $L = 1000$ m. Three different non-dimensional surface roughness lengths are used in the simulations, with values set at 10^{-4}, 2×10^{-4} and 5×10^{-4}, respectively. The computational domain is divided into $96 \times 96 \times 128$ uniformly spaced grid points; this yields a grid aspect ratio of $4 : 4 : 3/\pi$. The grid is staggered in the vertical direction, with the vertical velocity stored halfway between the other variables. The flow is driven by a constant pressure gradient in the streamwise direction with a non-dimensional magnitude of 0.5, while the velocity scale u_o used for normalization is taken to be 0.45 ms^{-1}.

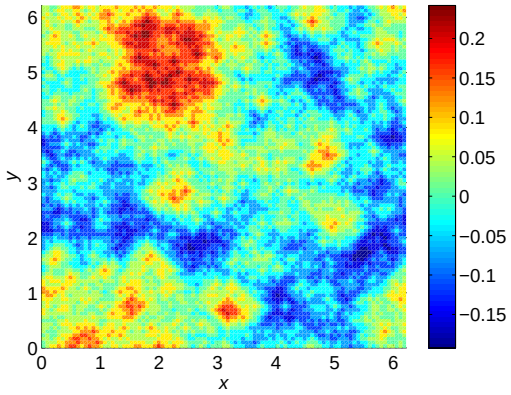

Figure 4.1: Multiscale complex terrain T_0 obtained using the RSOS model after 8×10^6 times. All dimensions have been normalized with a length scale of $L = 1000$ m.

.

Large-eddy simulations of ABL flow are performed over the terrains shown in Figure 4.3 and described in Table 1 (including a flat surface). Simulations are run for a period of time long enough to guarantee statistical convergence of the results;

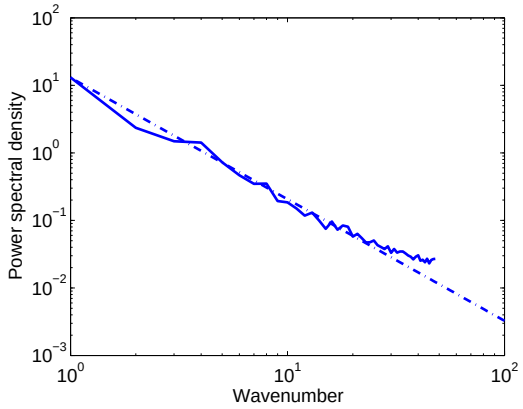

Figure 4.2: Elevation power spectral density of multiscale complex terrain T_0 against wavenumber (solid line). The dash-dot line show the -1.8 slope

the duration of the simulations is 2.67×10^5 s. The averaging period used in the simulations is the last 7.2×10^4 s of the simulation duration, with flow statistics presented and analyzed in the following section.

4.3 Results

Previous numerical [54, 79, 6] and experimental [71, 41,26] studies of flow over hills have shown that the area-averaged streamwise velocity varies logarithmically with height in the surface layer. Unlike the standard logarithmic law for neutral flow over homogeneous flat surfaces, which is based on the actual friction velocity (u_*) and the aerodynamic roughness of the surface (z_o), the logarithmic law for area-averaged velocity over hilly surfaces is formulated using an effective roughness length and an effective friction velocity. Therefore, the area-averaged velocity over complex topography can be written as

$$\langle u \rangle = \frac{u_*^{eff}}{\kappa} ln(\frac{z-d}{z_o^{eff}}), \tag{4.7}$$

where $\langle u \rangle$ is the area-averaged velocity over horizontal planes, u_*^{eff} is the effective friction velocity, κ is the von Karman constant, d is the effective displacement height, and z_o^{eff} is the effective roughness length. The effective friction velocity is equal to the square root of the total kinematic surface force (shear stress plus drag form) per unit area.

Previous studies (e.g., [79]) suggest that the effective displacement height is equal

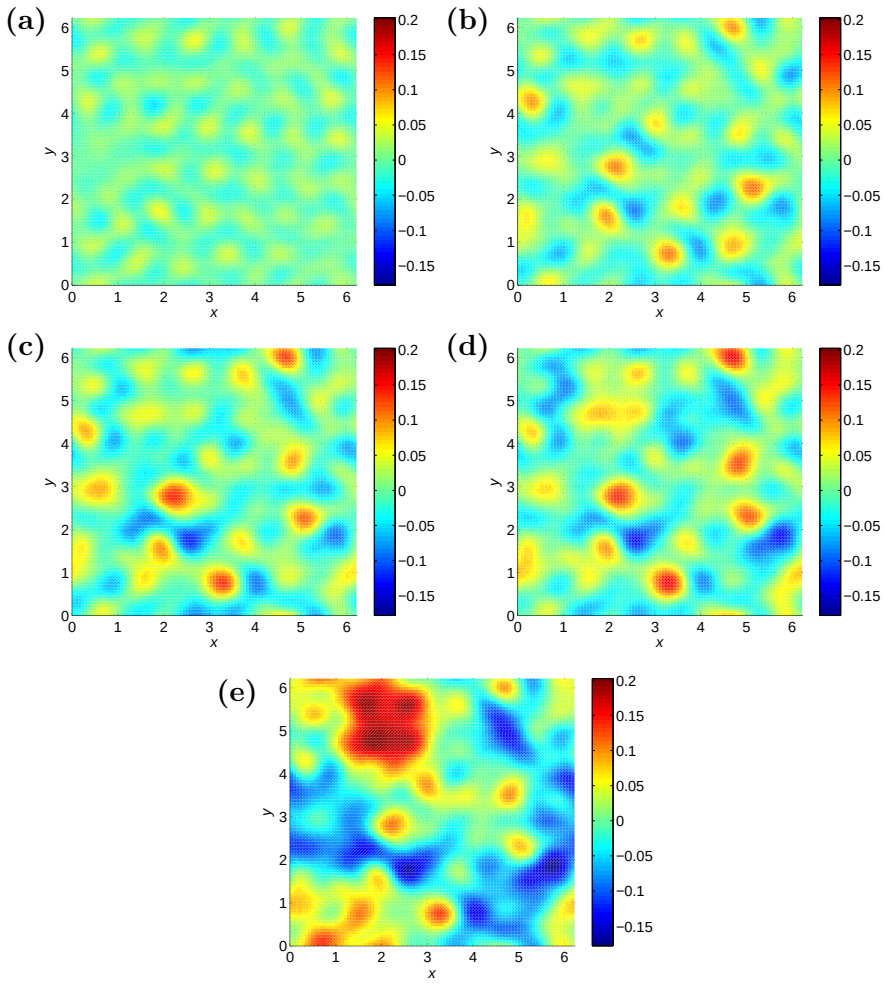

Figure 4.3: SGS terrains used as lower surfaces of the physical domain in LES: (a) T_1, (b) T_2, (c) T_3, (d) T_4, (e) T_5. All dimensions have been normalized with a length scale of $L = 1000$ m

to the mean height of surface elevation for hilly terrains. In the present study, all surfaces under consideration have a mean height of zero, making it reasonable for us to choose an effective displacement height of zero. Due to the constant pressure gradient exerted on the flow, the normalized simulated area-averaged total turbulent stress changes linearly with height, from a value of -1 at the surface to a value of zero at the top of the boundary layer. Consistent with that, the non-dimensional effective friction velocity u_*^{eff} has a value of 1.0 for all the simulations. Taking advantage of the known effective friction velocity u_*^{eff} as well as the area-averaged velocity $\langle u \rangle$ obtained from the simulations, and applying equation 4.7, we are able to determine the effective roughness length for all the different terrains under consideration.

The area-averaged non-dimensional velocity profiles from the simulations over the series of terrains considered here, with a non-dimensional surface roughness length of $z_o = 10^{-4}$, are shown in Figure 4.4 (a) to (f) with symbols. From those figures, we can see that all profiles show a logarithmic dependence with height in the surface layer, i.e., the lowest 15% of the domain. Knowing that the effective friction velocity u_*^{eff} is the same for all simulations, we can apply least squares fitting to the area-averaged velocity in the logarithmic region [6, 3] with straight lines of a constant slope of 2.5 ($= u_*^{eff}/\kappa$). The effective roughness length can then be obtained by finding the intercept of the straight fitted lines with the y-axis, where the average velocity is zero. The fitted lines are shown as solid lines in Figure 4.4 together with the coefficients of determination (R^2) obtained in the fitting. The SGS variance of elevation $\sigma_{h,sgs}^2$, surface roughness length z_o, computed effective roughness length z_o^{eff}, and the quantity $(z_o^{eff})^2 - z_o^2$ are listed in Table 2 for all terrains under consideration.

Figure 4.5 and Figure 4.6 show the area-averaged non-dimensional velocity profiles from simulations over the same series of SGS terrains, but now with non-dimensional surface roughness lengths of 2×10^{-4} and 5×10^{-4}, respectively. Again, in the lowest 10% - 15% of the domain, the velocity increases as the logarithm of height for all the simulations. Using the same least squares fitting method described above, the effective roughness lengths for the SGS terrains can be calculated. The obtained effective roughness values are shown in Table 2. From Figures 4.4, 4.5 and 4.6, we can see that the wind speed appears to gradually decrease with increasing orographic variance. Since the horizontal pressure gradient forcing is the same for all simulations, the area-averaged streamwise velocity increases against the logarithm of height at the same rate. For topography with larger orographic variance, however, the near-surface area-averaged streamwise velocity (at the same height) is smaller due to the larger total surface stress. This leads to a relatively smaller wind speed throughout the simulation domain. In order to illustrate the flow field generated by LES, we present in Figure 4.7 two sectional cuts of the streamwise velocity field over terrain T_5 with a non-dimensional surface roughness of 10^{-4}. Figure 4.7 (a) shows the time-averaged streamwise velocity field at the central vertical xz plane of the domain, and Figure 4.7 (b) presents the instantaneous streamwise velocity field at the same plane.

Next, we explore the relationship between the effective aerodynamic roughness and the SGS variance of the surface elevation. In particular, in order to evaluate the

validity of the simple linear model given by equation 4.5, the quantity $(z_o^{eff})^2 - z_o^2$ is plotted in Figure 4.8 against SGS variance of elevation $\sigma^2_{h,sgs}$ for the series of SGS terrains with the three different surface roughness lengths. From Figure 4.8, we can conclude that the linear relation between $(z_o^{eff})^2 - z_o^2$ and $\sigma^2_{h,sgs}$ holds true for most of the scales in all three cases. As mentioned above, it is reasonable that the increasing variance of surface elevation ($\sigma^2_{h,sgs}$) leads to an increase in the effective roughness length. For the three different surface roughness cases considered, that rate of increase (parameter C in equation 4.5) is shown to be constant over a wide range of scales. Only at the largest scale ($16\sqrt{2}\Delta$ in this study) does $(z_o^{eff})^2 - z_o^2$ no longer increase against $\sigma^2_{h,sgs}$ at the same rate as at smaller scales. Instead, our results show that those largest scales have practically no effect on the value of the effective roughness. In order to better understand the marginal effect of the largest scales, Figure 4.9 shows the elevation field obtained by low-pass filtering the initial multiscale terrain T_0 (Figure 4.1) with a filter of size $16\sqrt{2}\Delta$. The resulting filtered terrain is very mild and it is characterized by a maximum slope of 6 degrees. The fact that this range of scales (characterized by very mild slope) has little effect on the effective roughness z_o^{eff} of the surface is consistent with the simulation results of Wood and Mason [79]. They showed that, in simulations of flow over multiple 'packed' hills of the same size, the effect of the topography on the effective roughness height is very small (less than 20 percent increase with respect to the surface roughness) when the maximum slope of the terrain was smaller or equal to 6 degrees (see Table 1 in [79]).

In order to quantify the value of the parameter C in equation 4.5, i.e., the slope of the linear relation between $(z_o^{eff})^2 - z_o^2$ and $\sigma^2_{h,sgs}$ for the series of terrains considered here, we apply least squares fitting to the points within the linear scaling regions in Figure 4.8, and find the corresponding slope. The value of this slope is found to be 7×10^{-5}, 2×10^{-4} and 9×10^{-4} for the terrains with surface aerodynamic roughness z_o of 10^{-4}, 2×10^{-4} and 5×10^{-4}, respectively. It is therefore clear that the slope of the linear relation between $(z_o^{eff})^2 - z_o^2$ and $\sigma^2_{h,sgs}$ increases with increasing aerodynamic surface roughness length, a result that is supported by previous wind-tunnel studies performed over simple topographies. In particular, Gong et al. [25] showed that the two-dimensional sinusoidal hill with a relatively rough surface yielded a larger total drag (including both friction drag and form drag) than the same hill with a relatively smooth surface (see Table 2 in Gong et al. [25]). This indicates that, for a given topography, a larger surface roughness results in a larger total surface drag

as well as a larger effective roughness length.

In summary, our results confirm that the simple linear model given by equation 4.5 can be used to provide a reasonable estimation of z_o^{eff}, which can then be used in bulk similarity theory (the logarithmic law with effective parameters under neutral conditions) to estimate subgrid-scale turbulent momentum fluxes in numerical models of ABL flow over multiscale terrains. The proportionality parameter C is found to be constant for a given surface elevation field and aerodynamic roughness length z_o. For a given surface elevation field, the proportionality parameter increases with increasing roughness of the surface. It is worth pointing out that the proposed simple linear model (equation 4.5) also holds for different realizations of RSOS topography (not shown here), with the same value of the C coefficient.

4.4 Summary

It is known that the spectral density of elevation fields of many natural landscapes shows a -2 slope in a log-log scale over a wide range of spatial scales, from tens of kilometres down to metres (e.g., [64, 56]). This noteworthy scaling property led us to investigate its impact on surface momentum flux that results from the interaction between landscapes and the atmospheric boundary layer (ABL). Specifically, we examined how the effective roughness length of multi-scale subgrid-scale (SGS) topography (e.g., unresolved topography in coarser LES or high-resolution weather forecast models) relates to surface information of the topography such as the subgrid-scale variance of surface elevation. The multi-scale SGS topography is obtained from a landscape evolution model, the restricted solid-on-solid (RSOS) model [37]. LES with the tuning-free scale-dependent Lagrangian dynamic model [68] is used to perform numerical simulations of the ABL flow over a series of multi-scale SGS topography, and simulation results are used to examine the relation between the effective roughness length of multi-scale SGS topography and the subgrid-scale variance of surface elevation.

Large-eddy simulations of ABL flow over surface elevation fields containing different ranges of scales (considered SGS scales in larger scale numerical models) have been performed for three different aerodynamic surface roughness values z_o. The simulation results are used to calculate the resulting effective roughness length z_o^{eff} for each terrain (elevation field and surface roughness combination). By investigating the relation between the quantity $(z_o^{eff})^2 - z_o^2$ and SGS variance of elevation

$\sigma^2_{h,sgs}$, a clear scaling region has been identified for the series of topographies considered. The quantity $(z_o^{eff})^2 - z_o^2$ is found to increase linearly with the SGS variance of elevation as larger scales are considered, and it starts to converge at some large scale above which the multiscale terrain yields a very small maximum slope (about 6 degrees). The small effect of these scales, characterized by very mild slopes, is consistent with previous simulations results of flow over terrain with multiple hills of the same size. For a given surface elevation field, the magnitude of the slope C of the linear relation between $(z_o^{eff})^2 - z_o^2$ and $\sigma^2_{h,sgs}$, and therefore the value of the effective roughness length associated with a given terrain, is found to increase with increasing surface roughness of the terrain.

The linear relation between the square of the effective roughness length of multiscale subgrid-scale topography and the SGS variance of the surface elevation field reported in this study could be used in combination with bulk similarity theory (the logarithmic law with effective parameters under neutral stability conditions) to parametrize surface momentum fluxes from natural landscapes. Future research will focus on quantifying the value of the coefficient C as a function of terrain characteristics such as relative steepness of the terrain (e.g., maximum slope) and surface aerodynamic roughness of the surface. The value of C could also be computed dynamically with a procedure similar to the one recently proposed by Anderson and Meneveau [2] in the context of LES where the effects of the resolved topography are not explicitly represented by the numerical method (e.g., terrain-following coordinates), but parametrized using a drag model.

Table 1: The topographic statistics of lower surfaces of the LES physical domain

SGS terrain	Scales	SGS variance of elevation	Maximum height	Minimum height	Maximum slope
Flat	$4\sqrt{2}\Delta$ to $4\sqrt{2}\Delta$	0	0	0	0
T_1	$4\sqrt{2}\Delta$ to 8Δ	2.46E-04	0.0517	-0.0486	0.2539
T_2	$4\sqrt{2}\Delta$ to $8\sqrt{2}\Delta$	9.99E-04	0.1126	-0.0894	0.4510
T_3	$4\sqrt{2}\Delta$ to 16Δ	1.44E-03	0.1417	-0.1241	0.4983
T_4	$4\sqrt{2}\Delta$ to $16\sqrt{2}\Delta$	1.91E-03	0.1587	-0.1331	0.5161
T_5	$4\sqrt{2}\Delta$ to $32\sqrt{2}\Delta$	5.36E-03	0.2022	-0.1779	0.5603

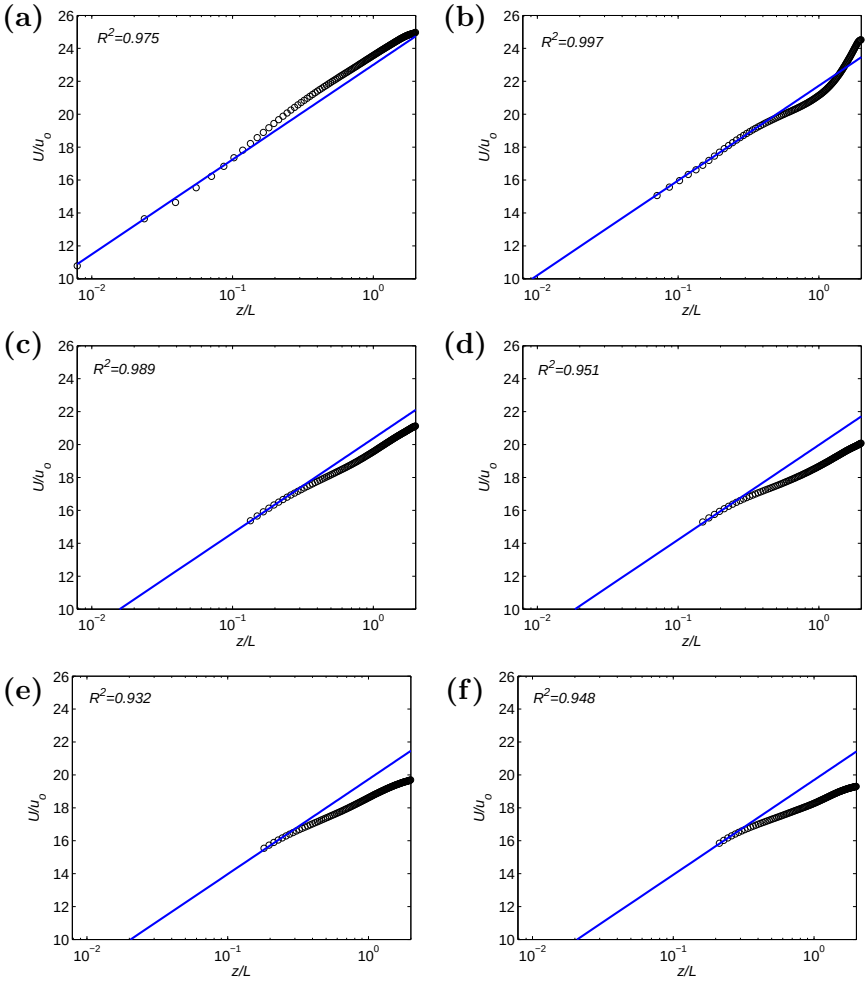

Figure 4.4: Area-averaged non-dimensional velocity profiles (shown in symbols) against height for the SGS terrains: (a) Flat terrain, (b) T_1, (c) T_2, (d) T_3, (e) T_4, (f) T_5. Least squares fitted lines for the lowest 15% part are also shown (solid lines). Non-dimensional surface roughness length for all the terrains is 10^{-4}. The coefficient of determination (R^2) from the linear regression in the surface layer is shown in all figures.

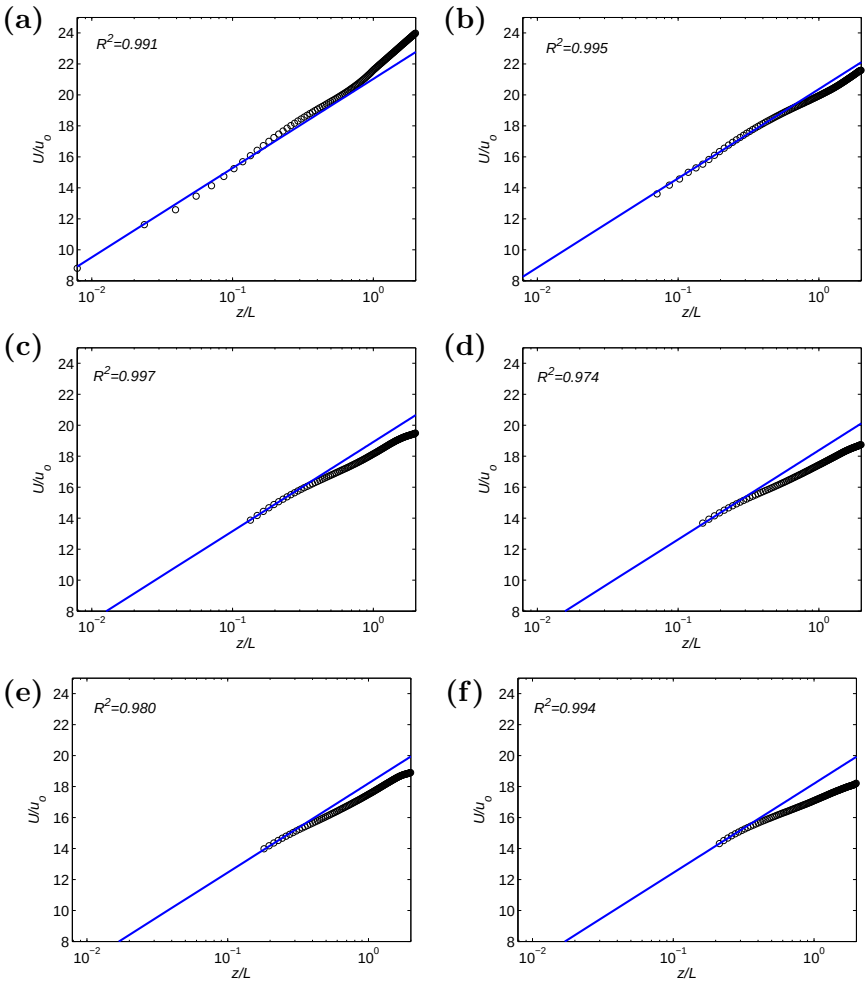

Figure 4.5: Area-averaged non-dimensional velocity profiles (shown in symbols) against height for the SGS terrains: (a) Flat terrain, (b) T_1, (c) T_2, (d) T_3, (e) T_4, (f) T_5. Least squares fitted lines for the lowest 15% part are also shown (solid lines). Non-dimensional surface roughness length for all the terrains is 2×10^{-4}. The coefficient of determination (R^2) from the linear regression in the surface layer is shown in all figures.

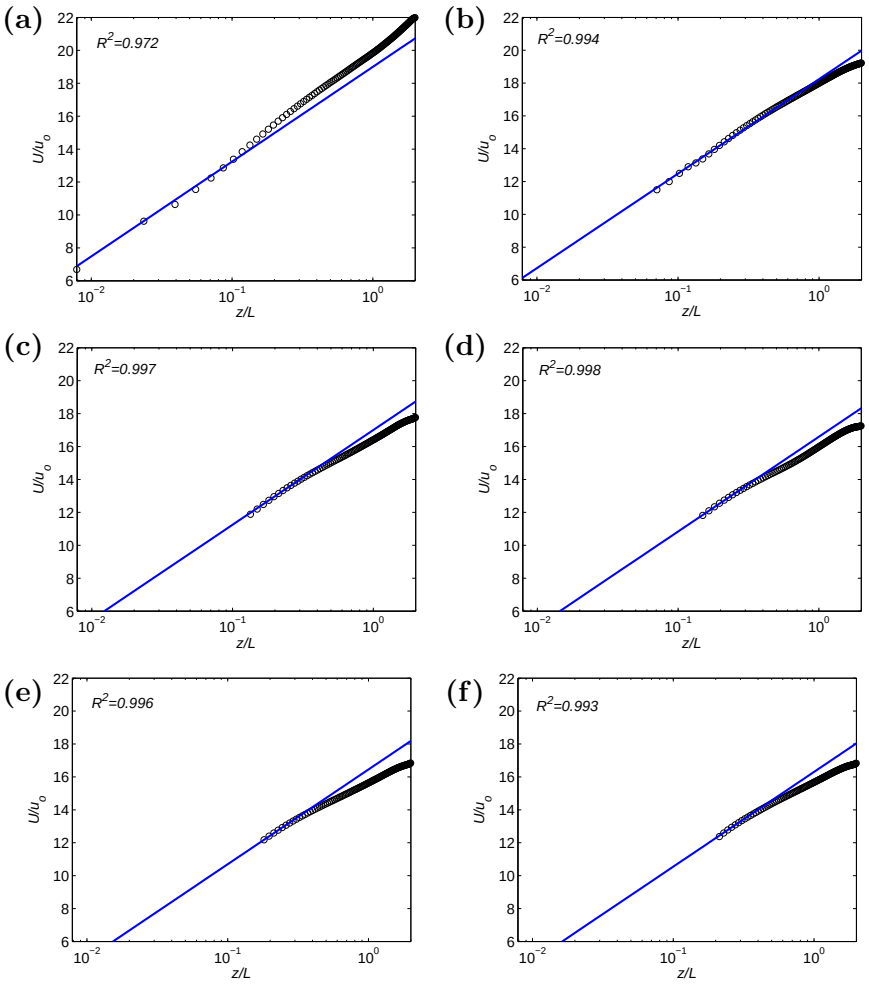

Figure 4.6: Area-averaged non-dimensional velocity profiles (shown in symbols) against height for the SGS terrains: (a) Flat terrain, (b) T_1, (c) T_2, (d) T_3, (e) T_4, (f) T_5. Least squares fitted lines for the lowest 15% part are also shown (solid lines). Non-dimensional surface roughness length for all the terrains is 5×10^{-4}. The coefficient of determination (R^2) from the linear regression in the surface layer is shown in all figures.

Table 2: SGS variance of elevation, surface roughness length, effective roughness length and an introduced quantity $(z_o^{eff})^2 - z_o^2$ for all the terrains under consideration

SGS terrain	Scales	SGS variance of elevation	surface roughness length	Effective roughness length	$(z_o^{eff})^2 - z_o^2$
Flat	$4\sqrt{2}\Delta$ to $4\sqrt{2}\Delta$	0	1.00×10^{-4}	1.00×10^{-4}	0
T_1	$4\sqrt{2}\Delta$ to 8Δ	2.46×10^{-4}	1.00×10^{-4}	1.75×10^{-4}	2.08×10^{-8}
T_2	$4\sqrt{2}\Delta$ to $8\sqrt{2}\Delta$	9.99×10^{-4}	1.00×10^{-4}	2.88×10^{-4}	7.28×10^{-8}
T_3	$4\sqrt{2}\Delta$ to 16Δ	1.44×10^{-3}	1.00×10^{-4}	3.37×10^{-4}	1.03×10^{-7}
T_4	$4\sqrt{2}\Delta$ to $16\sqrt{2}\Delta$	1.91×10^{-3}	1.00×10^{-4}	3.69×10^{-4}	1.26×10^{-7}
T_5	$4\sqrt{2}\Delta$ to $32\sqrt{2}\Delta$	5.36×10^{-3}	1.00×10^{-4}	3.77×10^{-4}	1.32×10^{-7}
Flat	$4\sqrt{2}\Delta$ to $4\sqrt{2}\Delta$	0	2.00×10^{-4}	2.20×10^{-4}	0
T_1	$4\sqrt{2}\Delta$ to 8Δ	2.46×10^{-4}	2.00×10^{-4}	3.03×10^{-4}	5.21×10^{-8}
T_2	$4\sqrt{2}\Delta$ to $8\sqrt{2}\Delta$	9.99×10^{-4}	2.00×10^{-4}	5.16×10^{-4}	2.26×10^{-7}
T_3	$4\sqrt{2}\Delta$ to 16Δ	1.44×10^{-3}	2.00×10^{-4}	6.37×10^{-4}	3.66×10^{-7}
T_4	$4\sqrt{2}\Delta$ to $16\sqrt{2}\Delta$	1.91×10^{-3}	2.00×10^{-4}	6.82×10^{-4}	4.25×10^{-7}
T_5	$4\sqrt{2}\Delta$ to $32\sqrt{2}\Delta$	5.36×10^{-3}	2.00×10^{-4}	6.89×10^{-4}	4.35×10^{-7}
Flat	$4\sqrt{2}\Delta$ to $4\sqrt{2}\Delta$	0	5.00×10^{-4}	5.00×10^{-4}	0
T_1	$4\sqrt{2}\Delta$ to 8Δ	2.46×10^{-4}	5.00×10^{-4}	7.19×10^{-4}	2.66×10^{-7}
T_2	$4\sqrt{2}\Delta$ to $8\sqrt{2}\Delta$	9.99×10^{-4}	5.00×10^{-4}	1.10×10^{-3}	9.60×10^{-7}
T_3	$4\sqrt{2}\Delta$ to 16Δ	1.44×10^{-3}	5.00×10^{-4}	1.30×10^{-3}	1.44×10^{-6}
T_4	$4\sqrt{2}\Delta$ to $16\sqrt{2}\Delta$	1.91×10^{-3}	5.00×10^{-4}	1.40×10^{-3}	1.71×10^{-6}
T_5	$4\sqrt{2}\Delta$ to $32\sqrt{2}\Delta$	5.36×10^{-3}	5.00×10^{-4}	1.50×10^{-3}	2.00×10^{-6}

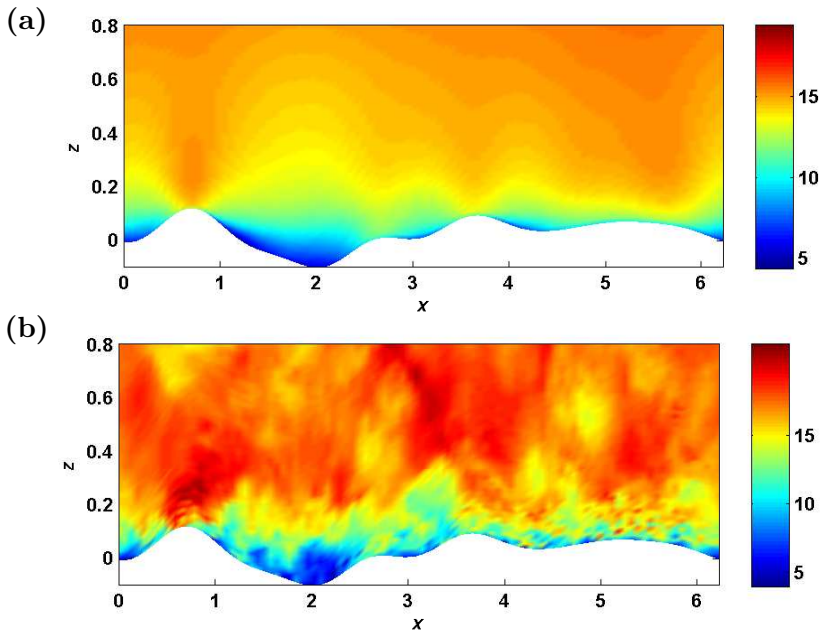

Figure 4.7: Non-dimensional streamwise velocity field generated by the large-eddy simulation over T_5 with a non-dimensional surface roughness of 10^{-4}: (a) time-averaged streamwise velocity field at the central vertical xz plane of the domain, (b) instantaneous streamwise velocity field at the same plane.

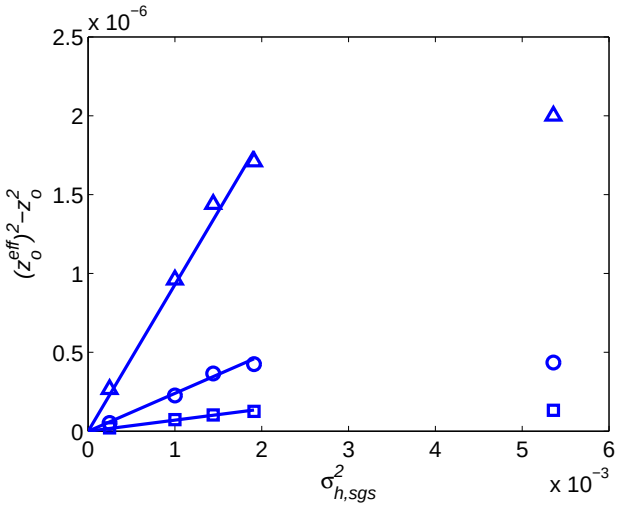

Figure 4.8: $(z_o^{eff})^2 - z_o^2$ versus $\sigma^2_{h,sgs}$ for the series of SGS terrains (shown in symbols): the squares denote results from SGS terrains with a non-dimensional surface roughness length of 10^{-4}, the circles denote results from SGS terrains with a non-dimensional surface roughness length of 2×10^{-4}, and the triangles denote results from SGS terrains with a non-dimensional surface roughness length of 5×10^{-4}. The solid lines are least squares fitted lines for the linear region.

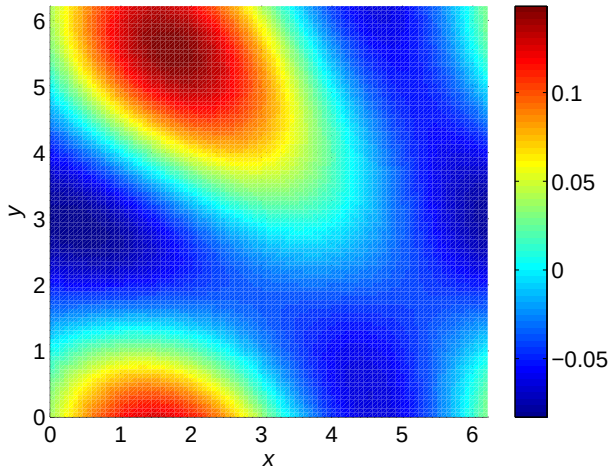

Figure 4.9: Elevation field above scale $16\sqrt{2}\Delta$ obtained from T

Chapter 5

Effective roughness of subgrid-scale topography in large-eddy simulation: A dynamic model

Abstract

Natural landscapes often exhibit mulstiscale self-similar characteristics, with a clear scaling and constant slope of the power spectrum of elevation over a wide range of scales, ranging from tens of kilometers to meters. As a result, in many large-eddy simulations (LESs) of atmospheric boundary layer (ABL) flow over multiscale complex terrain, the effect of the subgrid-scale (SGS) topography should be parameterized. In this study, LES is used to simulate neutrally-stratified ABL flow over multiscale complex terrain. The terrain is generated with a restricted solid-on-solid (RSOS) landscape evolution model, which is able to capture important statistical characteristics of natural landscapes, while assuring periodicity of the simulated fields consistent with the LES numerical methods. In order to study the effect of SGS topography in the LES, we filter the terrain and obtain a resolved topography that can be explicitly represented in LES, and a SGS topography, whose effect needs to be parameterized. The SGS topography effect is parameterized using an effective SGS roughness length, which is used in the lower boundary condition of the LES (the logarithmic law under neutral conditions). The effective SGS roughness length is formulated such that its square value grows linearly with the value of SGS variance of the filtered terrain. A dynamic model is introduced to compute the value of the proportionality coefficient C based on the application of the effective roughness model at two different scales, the topography filter scale and a slightly larger test-filter scale. By assuming scale invariance of the coefficient, the C value can be dynamically calculated during the simulation. We find the obtained C values at different scales are close to each other, which confirms our assumption of scale-invariance of the coefficient. The robustness of the proposed LES framework is

tested in simulations of ABL flow over a series of complex terrains that are filtered from the original terrain at various scales. Without using the effective roughness parameterization scheme, the area-averaged velocity profiles over the different filtered terrains show clear discrepancies. After including the model to obtain the C value and using the SGS roughness length in the surface boundary condition, the simulated velocity profiles show small dependence on resolution.

5.1 Introduction

Geomorphological processes (e.g., weathering, erosion, deposition, sedimentation) involved in landscape evolution are often characterized by variations in spatial and temporal scales. These processes leave their signatures on landscapes at different scales. As a result, natural landscapes exhibit multiscale (often multifractal) characteristics (e.g., [64]). When the same process acts across a range of scales, landscapes present self-similar (power-law scaling) properties across the scales. It is shown from both measured landscapes (e.g., [29]) and simulated landscapes (e.g., [56]) that power spectra of linear transects in natural landscapes often exhibit a log-log scaling range with a slope of -2 from tens of kilometers down to meters. As pointed out by Pelletier [57], the power-law scaling property observed in real topography is independent of the age of the landscape (time since significant uplift occurred) and the initial relief following tectonic uplift. This explains the universality of the power-law scaling properties that are found in many natural landscapes. This remarkable scaling property of surface elevation fields of natural landscapes motivates us to explore possible scaling properties related to surface momentum fluxes of the atmospheric boundary layer (ABL) flow over natural topography.

The effect of topography on turbulent transport in the ABL (e.g., momentum fluxes) has been a topic of numerous numerical studies (e.g., [70, 79]). Large-eddy simulation (LES) has become an increasingly popular tool to study turbulent flow over topography (e.g., [40, 73, 27, 10, 31, 74, 75]). It explicitly resolves eddies larger than the grid size and parameterizes smaller eddies using a subgrid-scale (SGS) model. By filtering the equations that govern the conservation of momentum, we obtain

$$\frac{\partial \widetilde{u}_i}{\partial x_i} = 0, \tag{5.1}$$

$$\frac{\partial \widetilde{u}_i}{\partial t} + \widetilde{u}_j(\frac{\partial \widetilde{u}_i}{\partial x_j} - \frac{\partial \widetilde{u}_j}{\partial x_i}) = -\frac{1}{\rho}\frac{\partial \widetilde{p}^*}{\partial x_i} - \frac{\partial \tau_{ij}}{\partial x_j} + F_i, \tag{5.2}$$

where the tilde represents the LES filtering operation, $\widetilde{u}_i$ is the filtered velocity in the i direction, x_i denotes the spatial coordinate in the i direction, t is time, ρ is air density, $\widetilde{p}^* = \widetilde{p} + \frac{1}{2}\rho\widetilde{u}_j\widetilde{u}_j$ is the modified pressure, $\widetilde{p}$ is the filtered pressure, F_i is a forcing term (e.g., a mean pressure gradient in the streamwise direction), and τ_{ij} denotes the SGS stress that needs to be parameterized using a SGS model.

The deviatoric part of the SGS stress is often parameterized using the eddy-viscosity model:

$$\tau_{ij} - \frac{1}{3}\delta_{ij}\tau_{kk} = -2\nu_{sgs}\widetilde{S}_{ij}, \tag{5.3}$$

$$\nu_{sgs} = [C_S\Delta]^2 \left|\widetilde{S}\right|, \tag{5.4}$$

where $\widetilde{S}_{ij} = \frac{1}{2}\left(\frac{\partial \widetilde{u}_i}{\partial x_j} + \frac{\partial \widetilde{u}_j}{\partial x_i}\right)$ is the resolved strain-rate tensor, ν_{sgs} is the eddy viscosity, the strain-rate tensor magnitude is calculated as $\left|\widetilde{S}\right| = \left(2\widetilde{S}_{ij}\widetilde{S}_{ij}\right)^{\frac{1}{2}}$, Δ is the size of the spatial filter, and C_S is the Smagorinsky coefficient.

LES results are found to be sensitive to the determination of model coefficients in SGS models. The specification of the Smagorinsky coefficient is therefore one of the biggest challenges when implementing the Smagorinsky model. For isotropic turbulence, if a cut-off filter falls within the inertial subrange, the value of C_S is known to be about 0.17 [42]. However, anisotropy of the flow, particularly the presence of a strong mean shear near the surface and around topography in high-Reynolds-number ABL flows, makes the optimum value of C_S depart from its isotropic counterpart (e.g., [68, 74, 75]).

To avoid the need for a priori specification or tuning of the model coefficient, Germano et al. [23] proposed the so-called dynamic procedure, which calculates the value of the model coefficient at every time and position in the flow based on information from the smallest resolved scales. In particular, it minimizes the error incurred when using the Smagorinsky model to compute the resolved Leonard stress (defined using a test filter scale, typically of size 2Δ) while assuming scale invariance of the coefficient in that range of scales. However, recent studies have shown that the assumption of scale invariance in the dynamic model can lead to errors in simulated boundary layer flows over both flat surfaces [61] as well as complex terrain [31, 74, 75].

By relaxing the assumption of scale invariance in the dynamic model, Porté-Agel et al. [61] proposed the scale-dependent dynamic model. In this model, two test filters of size 2Δ and 4Δ are introduced and used in the dynamic procedure, together with the assumption that the model coefficient has a power-law dependence with scale. When implementing the scale-dependent dynamic model, one needs to use some sort of averaging to guarantee numerical stability. Stoll and Porté-Agel [68] proposed the Lagrangian scale-dependent dynamic model, which employs Lagrangian averaging [49]. Lagrangian averaging consists of averaging over flow pathlines, which makes this model particularly suitable for simulations of non-homogeneous flows. Further details about the Lagrangian scale-dependent dynamic model can be found in Stoll and Porté-Agel [68].

The Lagrangian scale-dependent dynamic model has been tested, together with the Smagorinsky model [67] and the Lagrangian dynamic model [49] in simulating both neutral and stably-stratified boundary layer flow over simple topography like sinusoidal hills (e.g., [74, 75]). By comparing simulation results from the examined SGS models with turbulence statistics obtained in wind tunnel experiments, it is shown that the Lagrangian scale-dependent dynamic model [68] is able to yield more accurate flow statistics than the other two models due to its capability of capturing the scale dependence of the model coefficient associated with regions of the flow with strong shear. Therefore, in this study, we employ the Lagrangian scale-dependent dynamic model to parameterize SGS momentum fluxes in LES of neutral ABL over topography.

Despite the fact that the effect of topography on turbulent transport in the ABL has been extensively examined, most numerical studies have focused on the interactions between the ABL and topography with idealized shapes (e.g., sinusoidal hills). Few studies on the effect of multiscale complex topography on the ABL has been conducted. Previous studies (e.g., [57, 36]) have shown that one can numerically generate multiscale complex topography, which shares the same scaling properties as many natural landscapes (a -2 slope in elevation power spectrum in a log-log scale) and statistically makes a reasonable approximation to natural landscapes. The restricted solid-on-solid (RSOS) model [37] is one of those numerical techniques and often used to simulate landscape evolution (e.g., [57, 36]) and generate multiscale topography numrically. The model is proven to be equivalent to the Kardar-Parisi-Zhang (KPZ) equation [35] in the continuum limit [55]. It is worthy to note that, compared to some synthetic topography generation models that assume a Gaussian

probability distribution function (PDF) of topography, the RSOS model is able to generate more realistic topography because it can capture the skewness of the PDF of elevation found in natural landscapes. The topography of the earth's surface is highly skewed in a way that a much larger percentage of the total landscape is represented by lowlands (topography with an elevation smaller than the median elevation for a region) than highlands (topography with an elevation larger than the median elevation for a region). In the RSOS model, surface height of a two-dimensional lattice of uniformly distributed points is updated by random deposition, which is subject to the restriction that the elevation difference between any point and its nearest four neighboring points can only take the value of -1, 0 or 1. This restriction can prevent from generating surfaces with overhangs or vacancies. The random deposition process is repeated continuously until a steady-state condition is attained for which the surface height is equal to or greater than the linear dimension of the lattice. The elevation power spectra of the surfaces generated with the RSOS model show a power-law dependence on wave number with exponent close to -2 over a wide range of scales. This makes the surface a good approximation to natural landscapes (e.g., [29]).

In this research, we use LES with the Lagrangian scale-dependent dynamic model to study neutral ABL flow over multiscale complex topography. For the fine resolution multiscale complex topography generated from the RSOS model, we apply spatial filtering at some scale (typically several times the LES grid size) to the surface, so that it is separated into a resolved topography that can be represented directly in LES and a subgrid-scale (SGS) topography, whose effect needs to be parameterized in LES. An effective SGS roughness length is introduced for the SGS topography and is applied in the surface boundary condition (the logarithmic law under neutral conditions) in LES to parameterize the SGS topographic effect. The surface boundary condition is specified as

$$\tau_{xz} = -\frac{\kappa^2}{\ln^2(Z_m/z_o^{sgs})}\widetilde{V}(\widetilde{u}\ cos\theta_x + \widetilde{w}\ sin\theta_x), \tag{5.5}$$

$$\tau_{yz} = -\frac{\kappa^2}{\ln^2(Z_m/z_o^{sgs})}\widetilde{V}(\widetilde{v}\ cos\theta_y + \widetilde{w}\ sin\theta_y), \tag{5.6}$$

where τ_{xz} and τ_{yz} are the surface shear stresses at streamwise and spanwise directions, κ is the von Karman constant (=0.4), z_o^{sgs} is the effective SGS roughness length, Z_m is the reference height equal to the first computational model level height,

$\widetilde{u}$, $\widetilde{v}$ and $\widetilde{w}$ are the filtered streamwise, spanwise and vertical velocities, and $\widetilde{V}$ is the magnitude of the tangential velocity, all calculated at the lowest computational grid level. θ_x and θ_y are the local slopes of the topography in the x and y direction,.

The effective SGS roughness length z_o^{sgs} shown in equations 5.5 and 5.6 is proposed to be determined by an unknown dimensionless coefficient C, SGS elevation variance, and surface roughness length. It is calculated as

$$(z_o^{sgs})^2 - z_o^2 = C\sigma_{h,sgs}^2 = C\langle\widetilde{hh} - \widetilde{h}\widetilde{h}\rangle, \tag{5.7}$$

where z_o^{sgs} is the subgrid-scale (SGS) roughness length, z_o is surface roughness height, $\sigma_{h,sgs}^2$ is the SGS elevation variance which denotes the variance of elevation below a certain filter scale, h is surface elevation, and the tilde denotes spatial filtering at a certain scale, below which the SGS variance is computed. The value of the coefficient C is calculated dynamically in LES. Details of the dynamic calculation of the coefficient are introduced in the following part.

The drag that multiscale complex topography exerts on the ABL is composed of friction drag and form (pressure) drag. In terms of stress (drag per unit area), we know that the total stress includes surface shear stress and surface pressure. In this study, surface shear stress could be calculated based on a modified logarithmic law (surface boundary condition in LES, see equations 5.5 and 5.6), which employes a SGS roughness length for SGS topographic effect parameterization in LES. Surface pressure could be obtained directly from LES by solving the pressure Poisson equation. The total surface stress in the streamwise direction could therefore be obtained by computing and adding up the streamwise component of the surface shear stress and that of the surface pressure. As shown in equation 5.7, the dimensionless coefficient C appears in the SGS roughness length and is therefore incorporated in the formula for total stress (shown in equation 5.8). To determine this dimensionless coefficient C, we propose a dynamic type of model and introduce a filter scale Δ_1, which is the scale we used to filter the original fine-resolution multiscale complex topography to be used as the lower surface of the LES domain and a slightly larger test filter scale Δ_2. We are able to obtain the total surface stresses at both scales, which both contain the unknown coefficient C. At each time step in the simulation, by equating the area-averaged total stress at these two scales and assuming scale-invariance of the coefficient C, we are able to solve C dynamically in LES. The equation to be solved takes the following form:

$$\langle \frac{\widehat{u}^2\kappa^2}{(\ln \frac{z}{z_{o,1}^{sgs}})^2} \rangle_x + \langle \widehat{p_x} \rangle = \langle \frac{\widehat{\overline{u}}^2\kappa^2}{(\ln \frac{z}{z_{o,2}^{sgs}})^2} \rangle_x + \langle \widehat{\overline{p_x}} \rangle, \tag{5.8}$$

where hat and overbar denote spatial filtering at filter scale Δ_1 and test filter scale Δ_2, respectively, κ is the von Karman constant, p represents surface pressure obtained directly from simulations, subscript x denotes streamwise projection, $z_{o,1}^{sgs}$ is the SGS roughness length at the filter scale Δ_1, $z_{o,2}^{sgs}$ is the SGS roughness length at the test filter scale Δ_2. Both $z_{o,1}^{sgs}$ and $z_{o,2}^{sgs}$ contain the coefficient C when applying equation 5.7 at scales Δ_1 and Δ_2 respectively.

By solving equation 5.8 in LES at each time step, we are able to examine if the value of the coefficient C converges over time. We could also examine the proposed scale-invariance assumption of the coefficient by obtaining and comparing C values at different filter scales (LES resolutions). The validity of the SGS topographic effect parameterization scheme of using a SGS roughness length in the surface boundary condition of LES could be verified by comparing the area-averaged velocity profiles obtained from a series of simulations over multiscale complex terrains filtered at different filter scales (LES resolutions).

5.2 Numerical experiments

The multiscale complex topography used in this numerical study is obtained from the RSOS model [37]. The model simulates landscape evolution by starting from a flat two-dimensional lattice enforced with periodic boundary conditions. Random deposition is realized through randomly picking one point at a time and determining its new elevation by comparing its height with the height of neighboring points. Specifically, if the elevation at the chosen point is smaller than or equal to the elevation of its four neighboring points, the elevation of the point is increased by one, otherwise the elevation remains unchanged. The restriction is to ensure that the neighboring points should differ in height by no more than 1. In this way, we can keep updating the two-dimensional surface while avoid a surface with overhangs or vacancies until the surface elevation becomes equal to or greater than the linear dimension of the lattice. In this particular study, the two-dimensional lattice is of resolution 192×192. We updated the surface for 5×10^7 timesteps, and obtained a multiscale complex topography (not shown here). The topography is then shifted to a mean height of zero and scaled in all three directions to fit the LES domain

dimensions, which have non-dimensional values of 2π, 2π and 2. The resulting surface T_0 is presented in Figure 5.1. The power spectral of elevation field of the surface is plotted against wavenumber in a log-log scale (shown in Figure 5.2) and exhibits a clear -1.8 slope, which is very close to a -2 slope found in many natural landscapes (e.g., [29]).

We use two-dimensional spectral filters to spatially filter the obtained surface T_0 at the scale of 2, 4 and 8 times of T_0's grid resolution respectively. While performing the spectral filtering operation, the number of grid points of the surface is reduced accordingly by removing the filtered frequencies in the frequency domain. We therefore obtain three multiscale surfaces T_1, T_2 and T_3 with 96×96, 48×48 and 24×24 grid points (see Figure 5.3). In order to use the surfaces as the lower surface of LES domain, we spatially filter each of them again at 4 times of the surface's resolution and make the lower surface resolution 4 times of the LES resolution. The resulting surfaces (LES lower surfaces) are named T_{11}, T_{22} and T_{33} respectively and shown in Figure 5.4. The SGS elevation variance and maximum slope for each surface are presented in Table 5.1. Clearly, as shown in Table 5.1, SGS variance of elevation increases and maximum slope decreases as the surface resolution becomes lower. LESs are performed over the three surfaces, and for each surface, the corresponding SGS topographic effect is parameterized by using a SGS roughness length (see equation 5.7) in the surface boundary condition (the logarithmic law) of LES. In each simulation, the value of the coefficient C is calculated at every time step by solving the proposed model (equation 5.8). For the purpose of verifying the validity of the proposed parameterization scheme, LESs without including the SGS topographic effect are also performed over the three surfaces. Area-averaged streamwise velocity profiles are obtained and compared across simulations to verify the validity of the parameterization scheme.

A terrain following coordinate transformation [15] is employed to transform the physical domain to a rectangular computational domain. The length scale used in the simulations is 1000m, and velocity scale is set to be 0.45 ms^{-1}. The size of the computational domain, after being non-dimensionalized by the length scale is $2\pi \times 2\pi \times 2$, the dimensionless surface roughness length is 10^{-4}, the constant pressure gradient enforced in the streamwise direction to drive the ABL flow is 0.5, which yields a non-dimensional effective friction velocity of 1.0. For LES over surface T_{11}, T_{22},T_{33}, the computational domain is divided into $96 \times 96 \times 128$, $48 \times 48 \times 128$ and $24 \times 24 \times 64$ uniformly spaced grid points, respectively. The corresponding grid

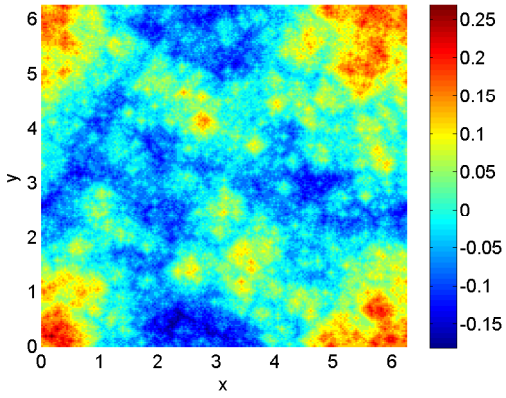

Figure 5.1: Multiscale complex terrain T_0 obtained from the RSOS model after 5×10^7 times. All dimensions have been normalized with a length scale of $L = 1000$ m.

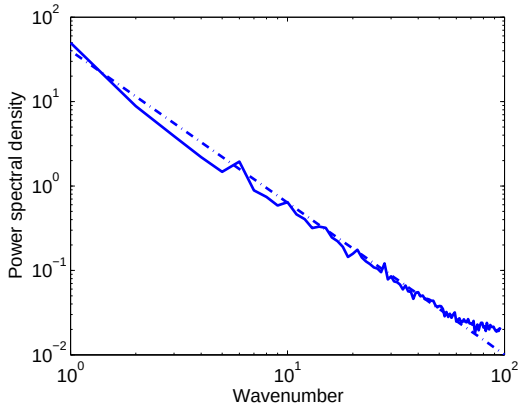

Figure 5.2: Elevation power spectrum of multiscale complex terrain T_0 against wavenumber (solid line). The dash-dot line show the -1.8 slope

aspect ratio is $4 : 4 : 3/\pi$, $8 : 8 : 3/\pi$, and $8 : 8 : 3/\pi$, respectively. The LES code used in this study is explained in Albertson and Parlange [1], Porté-Agel et al. [61], Stoll and Porté-Agel [68], Wan et al. [74], and Wan and Porté-Agel [75]. Periodic boundary conditions are enforced in the horizontal directions. The upper boundary is a fixed lid with vanishing vertical gradients (stress-free). The lower boundary condition applies the logarithmic law to calculate surface shear stress based on the horizontal velocities field at the lowest computational level. Spatial derivatives in the horizontal directions apply pseudospectral method, in the vertical direction, finite difference with second order accuracy is used. Time advancement is realized through the second-order Adams-Bashforth scheme. Simulations are run for a period of time

long enough to ensure quasi-steady flow conditions and statistical convergence of the results. Simulation results are presented in the following part.

5.3 Results

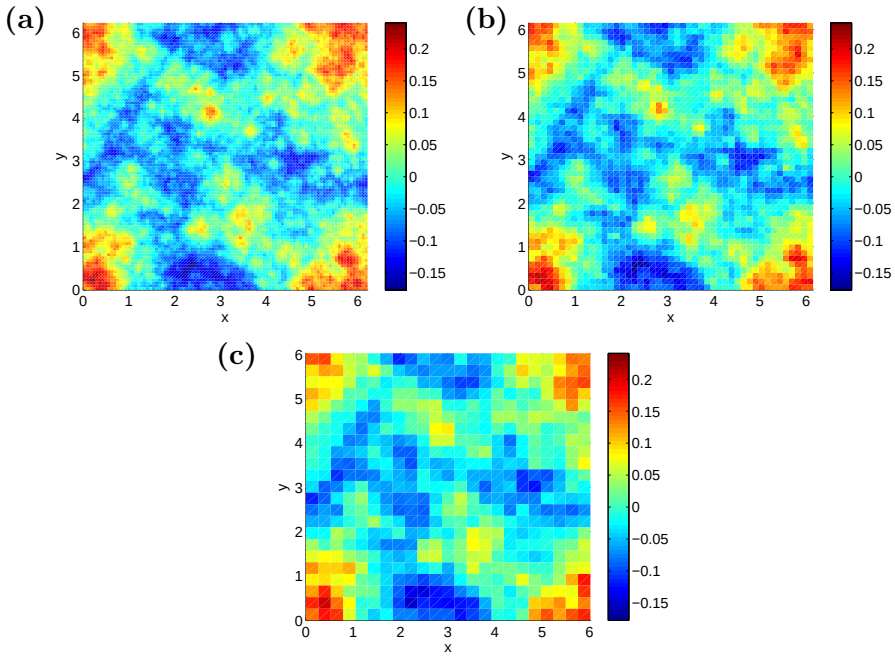

Figure 5.3: Topography spatially filtered from the initial complex terrain T_0 (Figure 5.1) using a spectral filter; grid resolution is reduced accordingly during the filtering operation: (a) T_1 with a resolution of 96×96, filtered at 2 times of T_0's grid resolution, (b) T_2 with a resolution of 48×48, filtered at 4 times of T_0's grid resolution, (c) T_3 with a resolution of 24×24, filtered at 8 times of T_0's grid resolution.

The dynamically obtained C value in each simulation is plotted against number of time steps and shown in Figure 5.5. We can see that the obtained C values at different scales are all fluctuating around the mean value of about 1.5×10^{-4}, which supports our scale-invariance assumption used when solving the C value from the model.

In order to validate the proposed SGS topographic effect parameterization scheme given by equations 5.5 and 5.6, we first run LESs over the three surfaces T_{11}, T_{22} and T_{33} (see Figure 5.4) without including the SGS topographic effect in LES. That is we specify the surface boundary condition in LES with the surface roughness

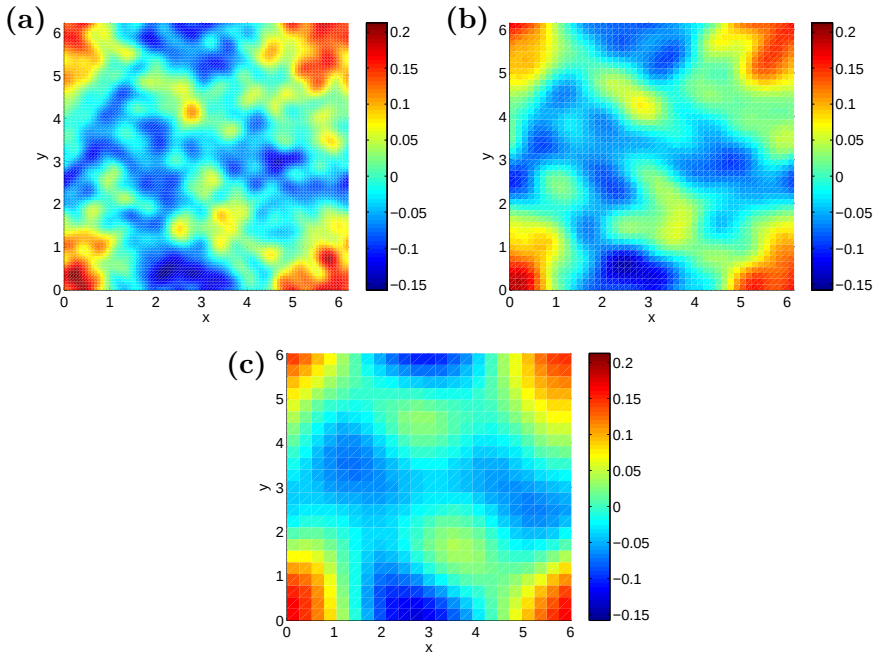

Figure 5.4: LES lower surfaces spatially filtered from terrains shown in Figure 5.3: (a) T_{11}, obtained from T_1 by filtering at 4 times of its resolution, (b) T_{22}, obtained from T_2 by filtering at 4 times of its resolution, (c) T_{33}, obtained from T_3 by filtering at 4 times of its resolution.

length z_0 (=0.1) instead of the SGS roughness length. The time and area-averaged streamwise velocity profiles against height are shown in Figure 5.6 (a). From Figure 5.6 (a), we can see that there are clear discrepencies among the profiles due to the differences of the three LES lower surfaces. By applying the SGS roughness length in the surface boundary condition and including the SGS topographic effect, we again plot the obtained time and area-averaged streamwise velocity versus height (shown in Figure 5.6 (b)). Comparing Figure 5.6 (a) and Figure 5.6 (b), we can

Table 5.1: SGS elevation variance and maximum slope of the LES lower surfaces

Surface	SGS elevation variance	Maximum slope
T_{11}	4.33×10^{-4}	0.520
T_{22}	8.21×10^{-4}	0.303
T_{33}	1.29×10^{-3}	0.131

see clearly that the profiles obtained by including the SGS topographic effect show less discrepancies than those obtained without the SGS topographic effect, which supports the proposed parameterization scheme as in equations 5.5, 5.6 and 5.7.

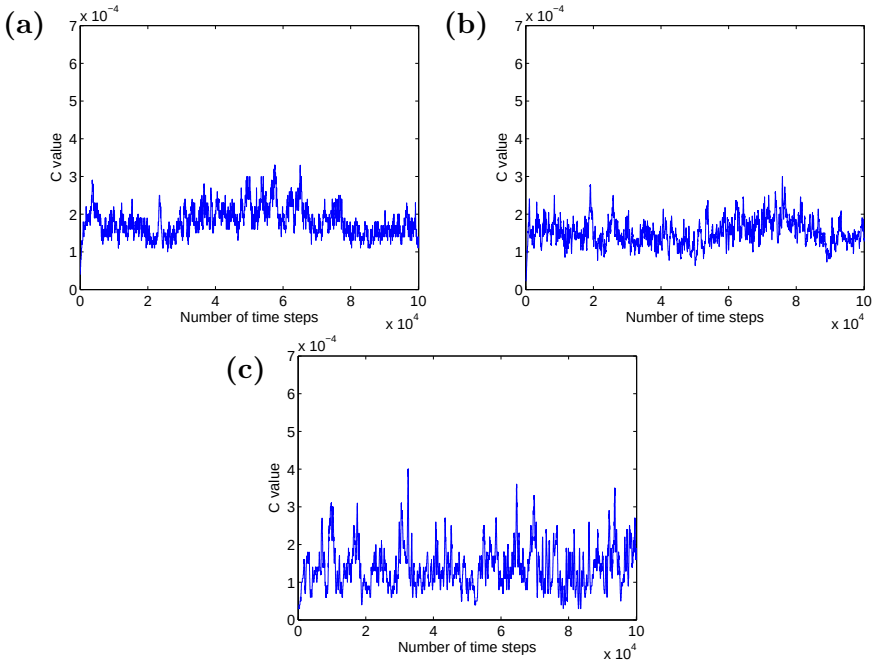

Figure 5.5: C value obtained dynamically in LES over topography against number of timesteps: (a) C value in LES over T_{11}, (b) C value in LES over T_{22}, (c) C value in LES over T_{33}.

5.4 Summary

Large-eddy simulation (LES) together with the Lagrangian scale-dependent dynamic model [68] has been used to simulate neutrally stratified atmospheric boundary layer (ABL) over multiscale complex topography, which is generated from the restricted solid-on-solid (RSOS) model and captures the scaling property of a -2 slope in elevation power spectrum in a log-log scale found in many natural landscapes. In order to represent the high-resolution multiscale complex surface in LES, a spatial filter is employed to separate the surface into two components. One is a resolved topography which can be directly used in LES. The other is a subgrid-scale (SGS) topography whose effect on the ABL needs to be modeled in LES. This SGS topographic effect is modeled in LES by using a SGS roughness length in the surface

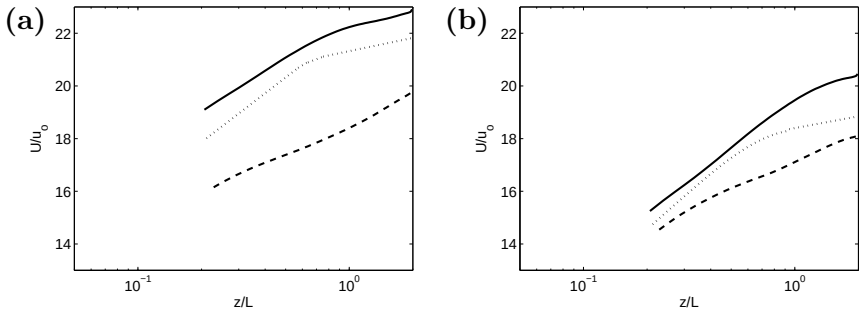

Figure 5.6: Time and area-averaged streamwise velocity profiles against height obtained from LES over different surfaces: surface T_{11} with 96×96 resolution (dashed lines), surface T_{22} with 48×48 resolution (dotted lines), surface T_{33} with 24×24 resolution (solid lines). Results are obtained from:(a) LES without using SGS parameterization, (b) LES using SGS parameterization.

boundary condition (the logarithmic law under neutral conditions). The SGS roughness length is proposed to be formulated with a SGS elevation variance, a surface roughness length and an unknown dimensionless coefficient C, which is dynamically computed in LES based on a proposed dynamic model (equation 5.8). In the model, one equates the streamwise component of the total surface stress at a filter scale and a slightly larger test filter scale, and assumes scale-invariance of the coefficient C. The coefficient could therefore be dynamically determined in LES.

LESs are performed over three different surfaces obtained from spatially filtering the initial fine-resolution multiscale complex topography generated from the RSOS model at various scales. The calculated coefficient C values are compared across the simulations and found to be close to each other, which supports the scale-invariance assumption made in this study. The proposed SGS topographic effect parameterization scheme is validated by comparing the time and area-averaged velocity profiles obtained from simulations with and without the SGS topographic effect parameterization. By replacing the surface roughness length with a SGS roughness length and taking the effect of SGS topography on the ABL into consideration, the obtained velocity profles clearly show more convergence than those obtained from simulations without SGS topographic effect parameterization, which means the proposed dynamic model to determine the C coefficient as well as the parameterization scheme are reasonable.

This study regarding the SGS topographic effect parameterization in LES is meaningful in that one can obtain reasonably good turbulent statistics of ABL

flow over high-resolution topography by simulating ABL flow over relatively simple filtered topography instead. It also has impact on regional scale parameterizations, which often require three-dimensional transient information on the ABL turbulence from LES over high-resolution complex terrain.

References

[1] J. D. Albertson and M. B. Parlange. Surface length scales in shear stress: Implications for land-atmosphere interactions over complex terrain. *Water Resources Res.* 35: 2121-2132, 1999.

[2] W. Anderson and C. Meneveau. Dynamic roughness model for large-eddy simulation of turbulent flow over multiscale, fractal-like rough surfaces. *J Fluid Mech* doi:10.1017/jfm.2011.137, 2011

[3] M. Athanassiadou and I. P. Castro. Neutral flow over a series of rough hills: a laboratory experiment. *Boundary-Layer Meteorol.*, 101:1-30, 2001.

[4] J. Bardina. (1983) *Improved turbulence models based on large eddy simulation of homogeneous, incompressible, turbulent flows.* PhD thesis; Stanford University, California, 1983.

[5] R. J. Beare, M. K. MacVean, A. A. M. Holtslag, J. Cuxart, I. Esau, J.-C. Golaz, M. A. Jimenez, M. Khairoutdinov, B. Kosovic, D. Lewellen, T. S. Lund, J. K. Lundquist, A. McCabe, A. F. Moene, Y. Noh, S. Raasch, and P. Sullivan. An intercomparison of large-eddy simulations of the stable boundary layer. *Boundary-Layer Meteorol.*, 118:247-272, 2006. DOI 10.1007/s10546-004-2820-6.

[6] S. Besio, A. Mazzino and C. F. Ratto. Local log-law of the wall: numerical evidences and reasons. *Phys. Lett. A* 275:152-158, 2000.

[7] E. Bou-Zeid, C. Meneveau and M. B. Parlange. Large-eddy simulation of neutral atmospheric boundary layer flow over heterogeneous surfaces: Blending height and effective surface roughness. *Water Resources Res.*, 40:1-18, 2004.

[8] E. Bou-Zeid, C. Meneveau, and M. B. Parlange. A scale-dependent Lagrangian dynamic model for large eddy simulation of complex turbulent flows. *Phys. Fluids*, 17, 2005. 025105.

[9] E. Bou-Zeid, N. Vercauteren, M. B. Parlange and C. Meneveau. Scale dependence of subgrid-scale model coefficients: An a priori study. *Phys. Fluids*, 20, 2008. 115106.

[10] A. R. Brown, J. M. Hobson and N. Wood. Large-eddy simulation of neutral turbulent flow over rough sinusoidal ridges. *Boundary-Layer Meteorol.* 98, 411-441. 2001.

[11] A. R. Brown and N. Wood. Properties and Parameterization of the Stable Boundary Layer over Moderate Topography. *J. Atmos. Sci.*, 60:2797-2808, 2003.

[12] R. J. Calhoun and R. L. Street. Turbulent flow over a wavy surface: Neutral case. it J. Geophys. Res., 106:9277-9293, 2001.

[13] R. J. Calhoun, R. L. Street and J. R. Koseff. Turbulent flow over a wavy surface: Stratified case. it J. Geophys. Res., 106:9295-9310, 2001.

[14] V. M. Canuto and Y. Cheng. Determination of the Smagorinsky-Lilly Constant C_S. *Phys. Fluids*, 9:1368-1378, 1997.

[15] T. Clark. A small-scale dynamic model using a terrain-following coordinate transformation. *J. Comp. Phys.*, 24:186-215, 1977.

[16] J. W. Deardorff. A numerical study of three-dimensional turbulent channel flow at large Reynolds numbers. *J. Fluid Mech.*, 41:453-480, 1970.

[17] J. W. Deardorff. On the Magnitude of the Subgrid-Scale Eddy Coefficient. *J. Comp. Phys.*, 7:120-133, 1971.

[18] J. W. Deardorff. Stratocumulus-Capped Mixed Layers Derived from a Three-Dimensional Model. *Boundary-Layer Meteorol.*, 18:495-527, 1980.

[19] A. C. De Vries, W. P. Kustas, J. C. Ritchie, W. Klaassen, M. Menenti, A. Rango, J. H. Prueger. Effective aerodynamic roughness estimated from airborne laser altimeter measurements of surface features. *Int. J. Remote Sens.*, 24:1545-1558, 2003.

[20] L. Ding, R. J. Calhoun and R. L. Street. Numerical simulation of strongly stratified flow over a three-dimensional hill. *Boundary-Layer Meteorol.*, 107:81-114, 2003.

[21] A. Dörnbrack and U. Schumann. Numerical simulation of turbulent convective flow over wavy terrain. *Boundary-Layer Meteorol.*, 65:323-355, 1993.

[22] K. A. Flack and M. P. Schultz. Review of Hydraulic Roughness Scales in the Fully Rough Regime. *J Fluids Eng*, doi:10.1115/1.4001492, 2010.

[23] M. Gernamo, U. Piomelli, P. Moin and W. Cabot. A dynamic subgrid-scale eddy viscosity model. *Phys. Fluids A*, 3(7):1760-1765, 1991.

[24] S. Ghosal, T. S. Lund, P. Moin and K. Akselvoll. A dynamic localization model for large-eddy simulation of turbulent flows. *J. Fluid Mech.*, 286:229-255, 1995.

[25] W. Gong, P. A. Taylor and A. Dörnbrack. Turbulent boundary- layer flow over fixed aerodynamically rough two-dimensional sinusoidal waves. *J. Fluid Mech.*, 312:1-37, 1996.

[26] A. L. M. Grant and P. J. Mason. Observations of boundary-layer structure over complex terrain. *Q. J. R. Meteorol. Soc.*, 116:159-186, 1990.

[27] D. S. Henn and R. I. Sykes. Large-eddy simulation of flow over wavy surfaces. *J. Fluid Mech.*, 383: 75-112, 1999.

[28] K. Horiuti. A proper velocity scale for modelling subgrid-scale eddy viscosities in large-eddy simulation. *Phys. Fluids A*, 5 (1):146-157, 1993.

[29] J. Huang and D. L. Turcotte. Fractal Mapping of Digitized Images: Application to the Topography of Arizona and Comparisons With Synthetic Images. *J. Geophys. Res.*, 94(B6):7491-7495, 1989.

[30] J. C. R. Hunt, D. D. Stretch and R. E. Britter. Length Scales in Stably Stratified Turbulent Flows and their Use in Turbulence Models. in J.S. Puttock (ed.), *Stably Stratified Flows and Gas Dynamics*, Clarendon Press, Oxford, 1988.

[31] S. Iizuka and H. Kondo. Performance of various sub-grid scale models in large-eddy simulation of turbulent flow over complex terrain. *Atmos. Environ.*, 38:7083-7091, 2004.

[32] S. Iizuka and H. Kondo. Large-eddy simulations of turbulent flow over complex terrain using modified static eddy viscosity models. *Atmos. Environ.*, 40:925-935, 2006.

[33] T. Ishihara and K. Hibi. An experimental study of turbulent boundary layer over a steep hill. Proceedings of the 15th National Symposium on Wind Engineering, 61-66, 1998.

[34] H. S. Kang and C. Meneveau. Universality of large eddy simulation model parameters across a turbulent wake behind a heated cylinder. *J. Turbul.*, 3:N32, 2002.

[35] M. Kardar, G. Parisi and Y. C. Zhang. Dynamic scaling of growing interfaces. *Phys. Rev. Lett.*, 56:889-892, 1986.

[36] H. J. Kim, I. M. Kim and J. M. Kim. River networks on the slope-correlated landscape. *Phys. Rev. E*, 62:3121-3124, 2000.

[37] J. M. Kim and J. M. Kosterlitz. Growth in a restricted solid-on solid model. *Phys. Rev. Lett.*, 62:2289-2292, 1989.

[38] J. Kleissl, V. Kumar, C. Meneveau and M. B. Parlange. Numerical study of dynamic Smagorinsky models in large-eddy simulation of the atmospheric boundary layer: Validation in stable and unstable conditions. *Water Resources Res.*, 42: W06D10, 2006.

[39] J. Kleissl, C. Meneveau and M. B. Parlange. On the Magnitude and Variability of Subgrid- Scale Eddy-Diffusion Coefficients in the Atmospheric Surface Layer. *J. Atmos. Sci.*, 60:2372- 2388, 2003.

[40] K. Krettenauer and U. Schumann. Numerical simulation of turbulent convection over wavy terrain. *J. Fluid Mech.*, 237:261-299, 1992.

[41] W. P. Kustas and W. Brutsaert. Wind profile constants in a neutral atmospheric boundary layer over complex terrain. *Boundary-Layer Meteorol.*, 34:35-54, 1986.

[42] D. K. Lilly. The representation of small-scale turbulence in numerical simulation experiments. In *In Proc. IBM Scientific Computing Symposium on Environmental Sciences*, page 195, White Plains, N. Y., 1967. IBM Data Process. Div.

[43] D. K. Lilly. A proposed modification of the Germano subgrid-scale closure method. *Phys. Fluids A*, 4(3):633-635, 1992.

[44] C. Maass and U. Schumann. Numerical simulation of turbulent convection over wavy terrain. Direct and Large-Eddy Simulation I, ed. by P.R. Voke, L. Kleiser and J.-P. Chollet, 287-297, Kluwer Academic, 1994.

[45] P. J. Mason and S. H. Derbyshire. Large-eddy simulation of the stably-stratified atmospheric boundary layer. *Boundary-Layer Meteorol.*, 53:117-162, 1990.

[46] P. J. Mason and R. I. Sykes. Flow over an isolated hill of moderate slope. *Quart. J. Roy. Meteorol. Soc.*, 105:383-395, 1979.

[47] P. J. Mason and D. J. Thomson. Stochastic backscatter in large-eddy simulations of boundary layers. *J. Fluid Mech.*, 242:51-78, 1992.

[48] C. Meneveau and T. S. Lund. The dynamic Smagorinsky model and scale-dependent coefficients in the viscous range of turbulence. *Phys. Fluids*, 9:3932-3934, 1997.

[49] C. Meneveau, T. S. Lund and W. Cabot. A Lagrangian dynamic subgrid-scale model of turbulence. *J. Fluid Mech.*, 319:353-385, 1996.

[50] S. F. Milton and C. A. Wilson. The impact of parameterized subgrid-scale orographic forcing on systematic errors in a global NWP model. *Mon. Weat. Rev.*, 124:2023-2045, 1996.

[51] P. Moin and J. Kim. Numerical investigation of turbulent channel flow. *J. Fluid Mech.*, 118:341-377, 1982.

[52] P. Moin, K. Squires, W. Cabot and S. Lee. A dynamic subgrid-scale model for compressible turbulence and scalar transport. *Phys. Fluids A*, 3(11):2746-2757, 1991.

[53] S. Murakami, A. Mochida, R. Ooka, S. Kato and Iizuka S. Numerical prediction of flow around a building with various turbulence models: comparison of k-ϵ EVM, ASM, DSM, and LES with wind tunnel tests. *Ashrae Trans.*, 102:741-753, 1996.

[54] T. J. Newley. *Turbulent airflow over hills.* Ph.D. dissertation, University of Cambridge, 1985.

[55] K. Park and B. N. Kahng. Exact derivation of the Kardar-Parisi-Zhang equation for the restricted solid-on-solid model. *Phys. Rev. E*, 51:796-798, 1995.

[56] P. Passalacqua, F. Porté-Agel, E. Foufoula-Georgiou and C. Paola. Application of dynamic subgrid-scale concepts from large-eddysimulation to modeling landscape evolution. *Water Resources Res.*, 42 W06D11, 2006.

[57] J. D. Pelletier. Why is topography fractal? arXiv:physics/9705033v1, 1997.

[58] J. D. Pelletier. Fractal behavior in space and time in a simplified model of fluvial landform evolution. *Geomorphology*, 91:291-301, 2007.

[59] U. Piomelli, P. Moin and J. H. Ferziger. Model consistency in large eddy simulation of turbulent channel flows. *Phys. Fluids*, 31:1884-1891, 1988.

[60] F. Porté-Agel. A scale-dependent dynamic model for scalar transport in large-eddy simulations of the atmospheric boundary layer. *Boundary-Layer Meteorol.*, 112:81-105, 2004.

[61] F. Porté-Agel, C. Meneveau and M. B. Parlange. A scale-dependent dynamic model for large-eddy simulation: application to a neutral atmospheric boundary layer. *J. Fluid Mech.*, 415:261-284, 2000.

[62] F. Porté-Agel, M. Pahlow, C. Meneveau and M. B. Parlange. Atmospheric Stability Effect on Subgrid-Scale Physics for Large-Eddy Simulation. Adv. Water Res., 24:1085-1102, 2001.

[63] F. Porté-Agel, M. B. Parlange, C. Meneveau and W. E. Eichinger. A priori field study of the subgrid-scale heat fluxes and dissipation in the atmospheric surface layer. *J. Atmos. Sci.*, 58:2673-2698, 2001.

[64] I. Rodriguez-Iturbe and A. Rinaldo. *Fractal River Basins*, Cambridge Univ. Press, New York, 1997.

[65] A. N. Ross, S. Arnold, S. B. Vosper, S. D. Mobbs, N. Dixon and A. G. Robins. A comparison of wind tunnel experiments and numerical simulations of neutral and stratified flow over a hill. *Boundary-Layer Meteorol.*, 113:427-459, 2004.

[66] U. Schumann. Subgrid Length-scales for Large-eddy Simulation of Stratified Turbulence. *Theor. Comp. Fluid Dyn.*, 2:279-290, 1991.

[67] J. Smagorinsky. General circulation experiments with the primitive equations: I. The basic experiment. *Mon. Weat. Rev.*, 91:99-164, 1963.

[68] R. Stoll and F. Porté-Agel. Dynamic subgrid-scale models for momentum and scalar fluxes in large-eddy simulation of neutrally stratified atmospheric boundary layers over heterogeneous terrain. *Water Resources Res.*, 42, W01409, 2006.

[69] R. Stoll and F. Porté-Agel. Large-eddy simulation of the stable atmospheric boundary layer using dynamic models with different averaging schemes. *Boundary-Layer Meteorol.*, 126:1-28, 2008.

[70] P. A. Taylor, R. I. Sykes and P. J. Mason. On the parametrization of drag over small-scale topography in neutrally-stratified boundary-layer flow. *Boundary-Layer Meteorol.*, 48:409-422, 1989.

[71] R. S. Thompson. Note on the aerodynamic roughness-length for complex terrain. *J. Appl. Meteorol.*, 17:1402-1403, 1978.

[72] Y. H. Tseng, C. Meneveau and M. B. Parlange. Modeling flow around bluff bodies and predicting urban dispersion using large eddy simulation. *Environ. Sci. Technol.*, 40:2653-2662, 2006.

[73] R. L. Walko, W. R. Cotton and R. A. Pielke. Large-eddy simulations of the effects of hilly terrain on the convective boundary layer. *Boundary-Layer Meteorol.*, 58:133-150, 1992.

[74] F. Wan, F. Porté-Agel and R. Stoll. Evaluation of dynamic subgrid-scale models in large-eddy simulations of neutral turbulent flow over a two-dimensional sinusoidal hill. *Atmos. Environ.*, 41:2719-2728, 2007.

[75] F. Wan, F. Porté-Agel. Large-eddy simulation of stably-stratified flow over a steep hill. *Boundary-Layer Meteorol.*, 138:367-384, 2010.

[76] J. K. Weissel, L. F. Pratson and A. Malinverno. The length-scaling properties of topography. *J. Geophys. Res.*, 99:13997-14012, 1994

[77] W. Weng, L. Chang, P. A. Taylor and D. Xu. Modelling stably stratified boundary layer flow over low hills. *Quart. J. Roy. Meteorl. Soc.*, 123:1841-1866, 1997.

[78] N. Wood, A. R. Brown and F. E. Hewer. Parametrizing the effects of orography on the boundary layer: An alternative to effective roughness lengths. *Quart. J. Roy. Meteorl. Soc.*, 127:759-777, 2001.

[79] N. Wood and P. J. Mason. The pressure force induced by neutral, turbulent flow over hills. *Quart. J. Roy. Meteorol. Soc.*, 119:1233-1267, 1993.

[80] M. V. Zagarola and A. J. Smits. Mean-flow scaling of turbulent pipe flow. *J Fluid Mech*, 373:33-79, 1998.